

# The planetary nebula Abell 48 and its [WN] nucleus

David J. Frew<sup>1,2\*</sup>, I.S. Bojičić<sup>1,2,3</sup>, Q.A. Parker<sup>1,2,3</sup>, M. Stupar<sup>1,2</sup>, S. Wachter<sup>4</sup>,  
K. DePew<sup>1,2</sup>, A. Danehkar<sup>1,2</sup>, M.T. Fitzgerald<sup>1,2</sup> and D. Douchin<sup>1,2</sup>

<sup>1</sup>*Department of Physics and Astronomy, Macquarie University, Sydney, NSW 2109, Australia*

<sup>2</sup>*Research Centre in Astronomy, Astrophysics & Astrophotonics, Macquarie University, Sydney, NSW 2109, Australia*

<sup>3</sup>*Australian Astronomical Observatory, PO Box 915, North Ryde, NSW 1670, Australia*

<sup>4</sup>*Spitzer Science Center, California Institute of Technology, MS 220-6, Pasadena, CA 91125, USA*

Accepted ; Received ; in original form

## ABSTRACT

We have conducted a detailed multi-wavelength study of the peculiar nebula Abell 48 and its central star. We classify the nucleus as a helium-rich, hydrogen-deficient star of type [WN4–5]. The evidence for either a massive WN or a low-mass [WN] interpretation is critically examined, and we firmly conclude that Abell 48 is a planetary nebula (PN) around an evolved low-mass star, rather than a Population I ejecta nebula. Importantly, the surrounding nebula has a morphology typical of PNe, and is not enriched in nitrogen, and thus not the ‘peeled atmosphere’ of a massive star. We estimate a distance of 1.6 kpc and a reddening,  $E(B - V) = 1.90$  mag, the latter value clearly showing the nebula lies on the near side of the Galactic bar, and cannot be a massive WN star. The ionized mass ( $\sim 0.3 M_{\odot}$ ) and electron density ( $700 \text{ cm}^{-3}$ ) are typical of middle-aged PNe. The observed stellar spectrum was compared to a grid of models from the Potsdam Wolf-Rayet (PoWR) grid. The best fit temperature is 71 kK, and the atmospheric composition is dominated by helium with an upper limit on the hydrogen abundance of 10 per cent. Our results are in very good agreement with the recent study of Todt et al., who determined a hydrogen fraction of 10 per cent and an unusually large nitrogen fraction of  $\sim 5$  per cent. This fraction is higher than any other low-mass H-deficient star, and is not readily explained by current post-AGB models. We give a discussion of the implications of this discovery for the late-stage evolution of intermediate-mass stars. There is now tentative evidence for two distinct helium-dominated post-AGB lineages, separate to the helium and carbon dominated surface compositions produced by a late thermal pulse. Further theoretical work is needed to explain these recent discoveries.

**Key words:** planetary nebulae: general – planetary nebulae: individual: Abell 48 – stars: Wolf-Rayet – stars: evolution

## 1 INTRODUCTION

Classical Wolf-Rayet (WR) stars are massive hydrogen-deficient objects with powerful, fast winds and high mass-loss rates up to  $10^{-4} M_{\odot} \text{ yr}^{-1}$  (Crowther 2007). Their spectra are characterised by strong, broad emission lines of helium, nitrogen, carbon or oxygen. A similar phenomenon is found in some ionizing stars of planetary nebulae (PNe), which descend from low mass progenitor stars and are unrelated in an evolutionary sense. These central stars (CSPNe) are denoted as [WR] stars, utilising the square brackets introduced by van der Hucht et al. (1985) to avoid confusion with their massive analogues. While massive WR stars are predominantly nitrogen or carbon enriched (WN or WC types respectively), with a few high temperature WO stars, almost all CSPNe catalogued to date belong

to the [WC]  $\rightarrow$  [WO] sequence (Tylenda et al. 1993; Crowther, De Marco & Barlow 1998; Acker & Neiner 2003), with one or two exceptions (e.g. Miszalski et al. 2012b, hereafter MC12).

In the course of a spectroscopic survey of detectable CSPNe (DePew et al. 2011), we were struck by the unusual nature of the nucleus of Abell 48 (PN G029.0+00.4), discovered and catalogued as a PN by Abell (1955, 1966). Abell 48 is a reddened, low-surface brightness PN with a morphology resembling a thick torus or cylinder, possibly viewed nearly pole-on (Figure 1). Abell (1966) classified it as a double-ring nebula<sup>1</sup> and gave an optical diameter of  $40''$ . It has not been well studied optically due to its relative faintness. DePew et al. (2011) already concluded that Abell 48 was a PN and gave a preliminary classification of the CSPN as [WN] or [WN/C],

\* E-mail: david.frew@mq.edu.au

<sup>1</sup> Curiously, Helfand et al. (2006) classified it as a candidate supernova remnant.

but since the important CIV  $\lambda 5806$  doublet was unobserved in that work, a more precise spectral type could not be determined. Independently, Wachter et al. (2010) classified the central source as a WN6 star, in contrast to the object's previous long association as a PN (Perek & Kohoutek 1967; Zuckerman & Aller 1986; Acker et al. 1992; Kohoutek 2001). This uncertainty led us to more closely investigate this interesting object and tie down its identification.

In this paper we present a detailed multi-wavelength study of Abell 48 and its CSPN, expanding on the preliminary analysis reported in Bojićić et al. (2013). As this paper was completed, an independent study of this object was published by Todt et al. (2013, hereafter TK13), coming to essentially the same conclusions as us. We will refer to their results in the context of our own paper where necessary. We have confirmed Abell 48's CSPN as a hydrogen-poor [WN] star, as first suggested by DePew et al. (2011). We also explore the nature and characteristics of the [WN] class based on a comparison of Abell 48 with the other [WN] and [WN/C] stars, their possible progenitors, and their likely progeny (Todt et al. 2010a,b, 2012; Werner 2012; MC12; TK13). This paper is arranged as follows: we describe our observations of Abell 48 in § 2, undertake a detailed analysis of the nebula and its CSPN in § 3 and § 4, and discuss the evidence for its nature in § 5. In § 6 we review the [WN] or [WN/C] classes, discuss the possible evolutionary pathways of these groups in § 7, before giving our conclusions and suggestions for future work in § 8.

## 2 OBSERVATIONS

### 2.1 Spectroscopic Observations

Optical spectra of Abell 48 and its CSPN were obtained on the ANU 2.3-metre telescope at Siding Spring Observatory using the Wide Field Spectrograph (WiFeS; Dopita et al. 2007, 2010), on 1 July 2009. WiFeS has a double-beam configuration, with spectral resolutions of 3000 or 7000, and a  $38'' \times 25''$  field of view with a spatial resolution of  $1''$ . Since the angular size of Abell 48 is larger than this, the instrument was positioned on the northern section of the nebula (including the CSPN) to make sure that some suitable background sky was available for subtraction. This was an early run during WiFeS commissioning time so the more effective nod-and-shuffle mode was not used. Low resolution gratings (B3000 and R3000) were employed and the exposure time on target was 1500s. Thin cloud was present during the observation.

Higher resolution gratings (B7000 and R7000) were used on a second run in April 2010. This observation was aimed at getting kinematic data on the nebula, so the IFU was positioned to cover both the CSPN and centre of the nebula. A further exposure of the southern section of the nebula was taken using WiFeS at low resolution in August 2012. The night was photometric and consequently the S/N ratio is best on this spectrum. For the WiFeS data, the frames were bias subtracted and flux- and wavelength-calibrated using the WiFeS data reduction pipeline (Dopita et al. 2010) in conjunction with standard IRAF routines. The flux calibration was performed using the spectrophotometric standard LTT 3864.

We also utilised the spectrum of the CSPN first presented by Wachter et al. (2010), obtained with the 5.0-m Hale telescope at Palomar Observatory on 4 September 2008 using the Double Spectrograph. This spectrograph also has a two-arm configuration, utilising a dichroic to split the light in to two channels, observed simultaneously. The 316 line  $\text{mm}^{-1}$  grating in first order, dichroic D55 and a slit width of  $1''$  were used. The resulting spectra cover

4000–5600 Å and 5800–8300 Å with a dispersion of 2.0 and 2.4 Å  $\text{pixel}^{-1}$  on the blue and red sides, respectively, with a spectral resolution of 5–7 Å. FeAr (blue) and HeNeAr (red) arcs were used for wavelength calibration. Bias and flat-field corrections to the raw spectrum images were performed using standard IRAF routines. A log of the observations is presented in Table 1.

### 2.2 Photometric Observations

New optical photometry of the CSPN was also obtained with the Australian National University's 2.3-m reflector at Siding Spring Observatory (SSO) in May 2012, and the 2.0-m Faulkes Telescope North (FTN) at Haleakala Observatory, Maui, in queue mode on three different nights in 2012. A log of the observations is presented in Table 1. The SSO observations used the standard imager at the f/18 Nasmyth focus. This used a  $2048 \times 2048$  pixel thinned E2V CCD with a pixel size is  $13.5 \mu\text{m}$ , giving a plate scale of  $0.34''/\text{pixel}$  across a  $6.6'$  circular field of view. Standard  $UBVI_c$  filters were used. The seeing was modest ( $\sim 1.5''$ ) and the night was photometric. Standard extinction coefficients were applied, and a range of standard stars from Landolt (2009) were measured to determine the colour equations used to convert from instrumental magnitudes. For the FTN observations, the Merope camera at the f/10 focus was used with  $BVI_c$  Johnson-Cousins filters. The camera utilised an E2V CCD with  $2048 \times 2048$  pixels, in  $2 \times 2$  binning mode, giving images  $4.7'$  on a side with a plate scale of  $0.28''/\text{pixel}$ . The averaged observed magnitudes are presented in § 4.1.

### 2.3 Archival Data

To supplement our spectroscopic and photometric data, we made an extensive search for archival multi-wavelength data of the nebula and central star using the Aladin Sky Atlas<sup>2</sup>, and the SkyView Virtual Observatory<sup>3</sup>. Narrowband H $\alpha$  (+ [N II]) images were obtained from the SuperCOSMOS H $\alpha$  Survey (SHS; Parker et al. 2005; Frew et al. 2013b) and the Southern H-Alpha Sky Survey Atlas (SHASSA) (Gaustad et al. 2001). Broadband images were also obtained from the SuperCOSMOS Sky Survey (SSS; Hambly et al. 2001), the 2MASS (Skrutskie et al. 2006) and UKIDSS (Lawrence et al. 2007) surveys in the near-IR, and the GLIMPSE (Benjamin et al. 2003; Churchwell et al. 2009), MIPS GAL (Carey et al. 2009), and WISE (Wright et al. 2010) mid-IR surveys.

Continuum fluxes for the nebula (and the CSPN separately if available), were retrieved from the VizieR service or measured from the original images as part of this work. We also downloaded 20 cm and 90 cm high-resolution MAGPIS images (Helfand et al. 2006) to supplement the NVSS radio data (Condon & Kaplan 1998). Figure 1 shows a multiwavelength montage of merged-colour images for Abell 48, all to the same scale. We adopt the best position for the CSPN from the 2MASS catalogue,  $\alpha = 18^{\text{h}} 42^{\text{m}} 46.92^{\text{s}}$ ,  $\delta = -03^{\circ} 13' 17.3''$  (J2000).

## 3 THE PLANETARY NEBULA

### 3.1 Nebular Morphology

Abell 48 has an apparent 'double-ring' morphology with a lozenge-shaped interior cavity (see Figure 1), which might be the projection

<sup>2</sup> Accessible from the Centre de Données Astronomiques (CDS).

<sup>3</sup> <http://skyview.gsfc.nasa.gov/>

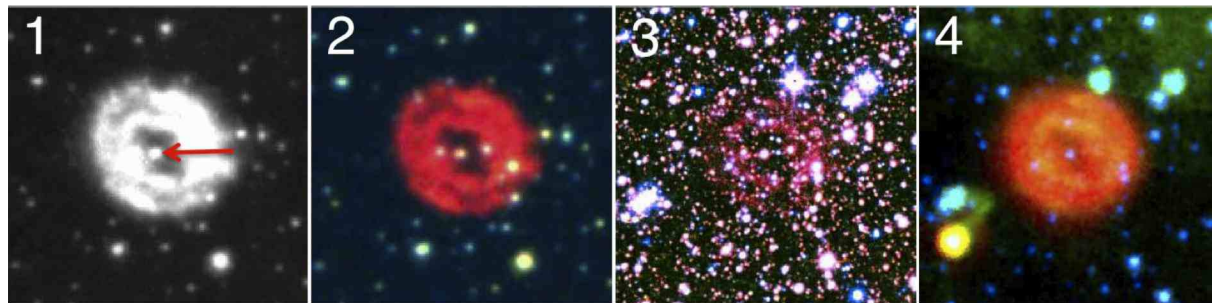


**Figure 1.** Montage of images for Abell 48, all to the same scale and orientation ( $90'' \times 90''$  with NE at top left), and with the colour palette set so that RGB channels map longer to shorter wavelengths respectively. 1. SHS  $H\alpha$  image with the CSPN marked – note the elliptical, double-ring structure of the nebula; 2. SSS/SHS composite  $B_J/R/H\alpha$  colour image; 3. UKIDSS  $JHK_s$  composite image; 4. IRAC/MIPS composite  $4.5/8.0/24 \mu\text{m}$  image. A colour version of this figure is available in the online journal.

**Table 1.** Spectroscopic and photometric observations of Abell 48 utilised in this study.

Date	Telescope	Instrument	$\lambda$ Range	$R = \lambda/\Delta\lambda$	Exp. time
2008 Sep 4	Hale 200-in	Dual Spectrograph	3400–5600, 5850–8300	1000	900
2009 Jul 1	ANU 2.3-m	WiFeS	3400–5900, 5300–9600	2900	1500
2010 Apr 22	ANU 2.3-m	WiFeS	4180–5580, 5300–7060	6900	1200
2012 Aug 23	ANU 2.3-m	WiFeS	3400–5900, 5300–9600	2900	1200
Date	Telescope	Instrument	Filter	...	Exp. time
2012 Feb 24	2.0-m FTN	Merope Camera	$B$	...	900
2012 Mar 14	2.0-m FTN	Merope Camera	$I_c$	...	10
2012 May 8	2.0-m FTN	Merope Camera	$BV$	...	200, 150
2012 May 18	ANU 2.3-m	Imager	$UBVI_c$	...	300, $2 \times 300$ , $2 \times 180$ , $2 \times 120$

of a thick torus or cylinder viewed nearly pole-on, as has been kinematically demonstrated for other morphologically similar nebulae (e.g. O’Dell et al. 2013). The measured dimensions from the SHS are  $44'' \times 39''$ . There is also a pair of point symmetric knots which are prominent in the  $[\text{N II}] \lambda 6584$  line (see Figure 2), and which are often seen in PNe. This fact, the PN-like morphology seen in  $H\alpha$  images, and the emission measure of the ionized nebula all indicate that it is material recently ejected by the CSPN, and not simply windswept interstellar material (see the morphological atlas of WR shells by Gruendl et al. 2000). This fact has important implications for the origin of the nebula, as we elucidate below.

Soker (1997) hinted that the CSPN of Abell 48 may be a binary system, based on nebular morphology (see later). If this turns out to be true, a binary evolution channel may be implicated to explain the unusual surface abundances of the CSPN, as has been suggested for the LMC PN, N 66 (Hamann et al. 2003) and for the peculiar CSPN of the Eskimo nebula, NGC 2392 (e.g. Méndez et al. 2012). The nebular emission-line profiles (see section 3.3.3, below) also appear to rule out simple spherical symmetry (cf. López et al. 2012), so we tentatively interpret the double shell morphology as due to the geometric orientation of two opposing lobes. A full morpho-kinematic analysis of the nebula, based on our WiFeS imaging data, will be the subject of a future paper, but a preliminary analysis indicates this is the likely scenario at play.

To the northwest of the PN there appear to be two faint closely spaced arcs about  $30''$  in extent, with the outermost being  $45''$  from the CSPN (see Figure 3). These arc-like structures were first noted by DePew (2011) and there also appears to be evidence of a very faint elliptical halo on deep continuum-subtracted SHS  $H\alpha$  images, discovered as part of the survey of Frew, Bojičić & Parker

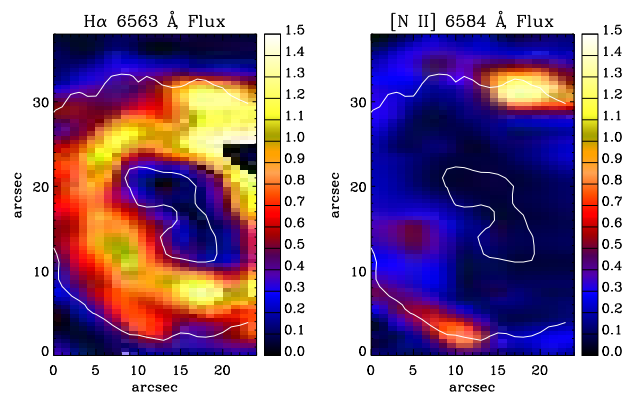


**Figure 2.** Surface brightness maps of Abell 48 in the  $H\alpha$  and  $[\text{N II}] \lambda 6584$  lines, extracted from the WiFeS observation of Apr 2010. Note the pair of opposing knots which are prominent in the  $[\text{N II}] \lambda 6584$  line. North-east is at top left in each panel and the flux units are in  $10^{-15} \text{ erg cm}^{-2} \text{ s}^{-1}$  per spaxel. A colour version of this figure is available in the online journal.

(2012)<sup>4</sup>. The overall dimensions are about  $280'' \times 210''$  in extent, but deep CCD images are needed to confirm them. Together, these features may provide evidence for earlier AGB mass-loss events. Even though Abell 48 is close to the Galactic mid-plane, where the interstellar medium (ISM) density is highest (Spitzer 1978), the PN has little signature of an ISM interaction (Soker, Borkowski & Sarazin 1991; Pierce et al. 2004; Wareing et al. 2006; Wareing 2010; Frew et al. 2011; Ali et al. 2012). Therefore the pecu-

<sup>4</sup> The SHS is an excellent search medium for faint structures surrounding PNe and symbiotic stars (see also Miszalski et al. 2012a).

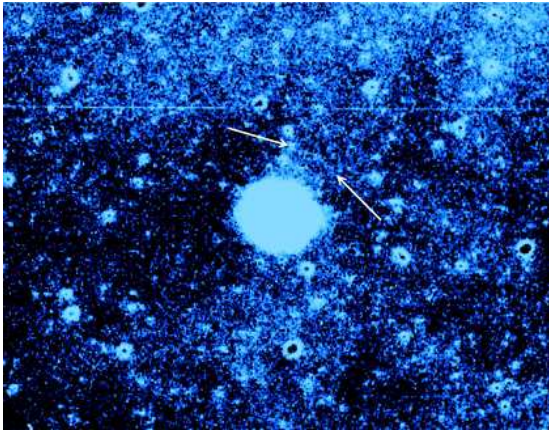


**Figure 3.** A deep continuum-divided ( $H\alpha$ ) SHS image of Abell 48 showing two short arcs, the outer one arrowed, located  $35''$  and  $45''$  north-west of the CSPN. The image subtends  $300'' \times 240''$  with NE at top left.

liar velocity of the CSPN is likely to be low ( $<40 \text{ km s}^{-1}$ ). In contrast, TK13 claim Abell 48 is a runaway star, based on the CSPN’s proper motion of  $19.5 \text{ mas yr}^{-1}$  in p.a.  $222^\circ$  from the PPMXL catalogue (Roeser, Demleitner & Schilbach 2010). However, this differs from the USNO-B1.0 catalogue value (Monet et al. 2003) of  $25.3 \text{ mas yr}^{-1}$  in p.a.  $342^\circ$ . Owing to the faintness of the star, these catalogue values may be spurious.

### 3.2 Integrated Nebular Fluxes

We have four independent estimates of the integrated  $H\alpha$  flux. Frew et al. (2013a) derived  $\log F(H\alpha) = -11.52 \pm 0.09$  (in cgs units) from aperture photometry on SHASSA images, while Frew et al. (2013b) estimated  $\log F(H\alpha) = -11.56 \pm 0.15$  from newly-calibrated SuperCOSMOS  $H\alpha$  images, in good agreement. We also used our WiFeS data, scaling up the fluxes to account for the portion of the nebula that was not observed. We did this for two separate runs to obtain  $\log F(H\alpha) = -11.59$  and  $-11.62$  respectively. The weighted mean flux is  $\log F(H\alpha) = -11.58 \pm 0.06 \text{ erg cm}^{-2} \text{ s}^{-1}$ , adopted hereafter.

In the radio-continuum domain we found two catalogued but discrepant values for the 1.4 GHz (20 cm) integrated flux density of Abell 48;  $S_{1.4} = 159 \pm 15 \text{ mJy}$  from the NRAO VLA Sky Survey (NVSS; Condon et al. 1998; Condon & Kaplan 1998) and  $S_{1.4} \approx 657 \text{ mJy}$ , catalogued in the Multi-Array Galactic Plane Imaging Survey (MAGPIS; Helfand et al. 2006). The discrepancy is too large to be attributed to confusion by the complex background, as noted by Condon & Kaplan (1998). Therefore, we re-measured the flux density from the MAGPIS and NVSS total intensity images<sup>5</sup> using the KARMA data analysis package (Gooch 1996). While our estimated flux density from the NVSS image agrees with the catalogued value within the uncertainties, we measured a flux of  $\sim 200 \text{ mJy}$  from the MAGPIS image, at odds with the catalogued value, but closer to the NVSS flux. In fact some published MAGPIS fluxes need to be revised (D. Helfand, 2011, private communication), and the catalogued value of  $657 \text{ mJy}$  is erroneous in this case. Abell 48 is not detected in the high-resolution Coordinated

**Table 2.** Summary of continuum flux measurements for Abell 48.

Wavelength ( $\mu\text{m}$ )	Flux (mJy)	Survey	Reference
3.6	$67 \pm 7$	IRAC	C11
4.5	$109 \pm 10$	IRAC	C11
5.8	$32 \pm 5$	IRAC	C11
8.0	$244 \pm 24$	IRAC	C11
8.3	$375 \pm 15^a$	MSX	EP03
11.6	$1195 \pm 120$	WISE	This work
14.7	$2053 \pm 125$	MSX	EP03
18	$3341 \pm 42$	AKARI	I10
21.3	$1735 \pm 110$	MSX	EP03
22.1	$1600 \pm 200$	WISE	This work
24	$2065 \pm 100$	MIPSGAL	M10, PM11
25	$2530 \pm 250$	IRAS	IPAC
60	$<2070$	IRAS	IPAC
65	$29020 \pm 570^a$	AKARI	I10
70	$11000 \pm 2000$	MIPSGAL	This work
90	$30990 \pm 2200^a$	AKARI	I10
6 cm	$>70$	MAGPIS	This work
6 cm	$<400$	NVSS	This work
11 cm	$\geq 220$	VLA	PB03, this work
20 cm	$159 \pm 15$	NVSS	C98
20 cm	$200 \pm 20$	MAGPIS	This work
90 cm	$60 \pm 10$	MAGPIS	This work

References: C11 – Cohen et al. (2011); C98 – Condon et al. (1998); EP03 – Egan et al. (2003); I10 – Ishihara et al. (2010); IPAC – IPAC (1986); M10 – Mizuno et al. (2010); PB03 – Paladini et al. (2003); PM11 – Phillips & Marquez-Lugo (2011); <sup>a</sup> Fluxes likely confused with surrounding emission.

Radio and Infrared Survey for High-mass Star Formation (CORNISH) Source Catalog (Purcell et al. 2013), recently undertaken at 5 GHz with the Very Large Array (VLA). Abell 48 is just below the survey sensitivity threshold and is likely resolved out by the  $uv$ -coverage of the VLA B-configuration (C. Purcell, 2013, priv. comm.). The resolution of the MAGPIS image allows us to filter out the features close to Abell 48 and so avoid the confusion problem which affects the older NVSS data. Hence, we use our new measurement for further analysis. In addition, we measured the flux density at 0.325 GHz (90 cm) from an intensity image taken as a part of the MAGPIS survey (for more details see Helfand et al. 2006). Both flux values are tabulated in Table 2, along with several additional integrated flux measurements of the nebula taken from the literature. It is clearly seen from these fluxes that the emission from the nebula is thermal in nature, typical of photoionized gas.

#### 3.2.1 Infrared Fluxes

These are several flux determinations at infrared (IR) wavelengths. The nebula is faint in 2MASS and UKIDSS images. In the  $K_s$  band, which has the strongest detection, we attribute the flux to molecular hydrogen ( $H_2$ ) at  $2.12 \mu\text{m}$ , as well as the  $\text{Br}\gamma$   $2.17 \mu\text{m}$  hydrogen line (Kimeswenger et al. 1998). The GLIMPSE data resolves the nebula well, and it appears brightest in the IRAC2 and IRAC4 bands. On this basis, the  $\text{Br}\alpha$   $4.05 \mu\text{m}$  line is probably the strongest feature contributing to the IRAC2 flux, and strong polycyclic aromatic hydrocarbon (PAH) bands (Allamandola, Tielens & Barker 1989) likely contribute to the IRAC4 flux, particularly the bands at  $7.7$  and  $8.6 \mu\text{m}$ , with some emission from  $\text{P}\text{f}\alpha$   $7.46 \mu\text{m}$  and the  $[\text{Ar III}]$   $8.99 \mu\text{m}$  fine-structure line. We ran a preliminary photoionization model to test these predictions using the

<sup>5</sup> The images were retrieved from the NVSS and MAGPIS postage stamp servers: <http://www.cv.nrao.edu/nvss/> and <http://third.ucllnl.org/gps/>

three-dimensional photoionization code MOCASSIN (Ercolano et al. 2003, 2005). This predicts an [Ar III] 8.99 $\mu$ m line flux of around 20% of H $\beta$ . A full analysis will be published separately.

Abell 48 is prominent in the WISE3 (11.6 $\mu$ m) and WISE4 (22 $\mu$ m) bands, but only barely seen in WISE2. Features that may contribute to the WISE3 band are PAH emission, particularly at 11.3 $\mu$ m, thermally-emitting dust, and the [S IV] 10.5 $\mu$ m line which our photoionization model suggests is comparable in strength to H $\beta$ . Other predicted contributors, in order of decreasing strength, are the [Ar III] 8.99 $\mu$ m, [Ne III] 15.5 $\mu$ m, and [Ne II] 12.8 $\mu$ m lines. Similarly, it is a moderately strong source in the MIPS 24 $\mu$ m band (Mizuno et al. 2010; Wachter et al. 2010), considering that the [O IV] fine-structure line is expected to be weak or absent in a nebula of this excitation class. In fact our optical spectra (Figure 5) show no emission lines with an ionization potential (I.P.) exceeding 41.0 eV, based on the weak detection of the [Ne III]  $\lambda$ 3869 line. This suggests that warm dust is the main contributor to the 22 and 24 $\mu$ m bands, with a likely minor contribution from the [Ar III] 21.81 $\mu$ m line. The spectral energy distribution (SED) of the nebula, not shown here, is dominated by this dust component. From a blackbody fit to the IR fluxes given in Table 2 we estimate a dust temperature of 150 K, quite typical of PNe. Mizuno et al. (2010) also found that the nebular 8 $\mu$ m emission was co-spatial with the 24 $\mu$ m emission. Similarly, we find the angular size to be similar at all wavelengths indicating that the ionized, molecular, and dust components are spatially mixed. The IRAC/MIPS false-colour image<sup>6</sup> (Figure 1) illustrates this. A summary of all nebular continuum fluxes is given in Table 2.

### 3.3 Nebular Spectroscopy

Our three WiFeS data cubes were used to investigate the nebular conditions. Figure 4 presents individual slices of the low-resolution ( $R = 3000$ ) and medium-resolution ( $R = 7000$ ) WiFeS red-arm spectra respectively. The broad features from the CSPN, the respective nebular and night sky line strengths, and line-splitting of the nebular lines due to expansion can be seen. The 1-D low-resolution spectrum from 2012, binned from the data cube to increase the signal to noise (S/N) ratio, is illustrated in Figure 5. It shows the presence of a bright nebular H $\alpha$  line and relatively weak [N II]  $\lambda$ 6548,84 lines in the red ([N II]/H $\alpha$  = 0.28), a steep Balmer decrement due to the relatively high extinction, as well as fairly weak [O III] lines in the blue relative to H $\beta$ . There is no indication of a nebular He II  $\lambda$ 4686 line (to a level of 1% percent of H $\beta$ ).

In Table 3, we summarise the observed and reddening-corrected line fluxes. The other WiFeS spectra were used to confirm that the faintest nebular lines were real. The spectrum presented by TK13 is similar to our own, the main difference being that TK13 estimated a somewhat higher extinction. Abell 48 has a low excitation class, EC = 1.45 (Dopita & Meatheringham 1990; Reid & Parker 2010), so we conclude that the weak  $\lambda$ 7236 feature that we also detected is more likely to be a C II recombination line rather than the [Ar IV] line on the basis of our photoionization model.

#### 3.3.1 Reddening

A summary of the various reddening determinations is presented in Table 4. We derived the logarithmic extinction at H $\beta$ , and hence

**Table 3.** List of emission line fluxes for Abell 48, adopted from the high S/N WiFeS IFU spectrum from 2012.

Line	$\lambda$	$f(\lambda)$	$F(\lambda)$	$I(\lambda)$
[O II]	3727	0.256	13:	64:
[Ne III]	3869	0.230	6.8:	28:
H $\delta$	4101	0.182	6.6:	20:
H $\gamma$	4340	0.127	19.9	43.5
[O III]	4363	0.121	<1.0	<2.1
He I	4471	0.095	5.0:	9.0:
He II	4686	0.043	<0.8	<1.0
H $\beta$	4861	0.000	100	100
[O III]	4959	-0.024	119	103
[O III]	5007	-0.036	402	322
[N II]	5755	-0.195	1.3:	0.40:
He I	5876	-0.215	67.6	17.9
[S III]	6312	-0.283	2.1:	0.37:
[N II]	6548	-0.318	138	19.4
H $\alpha$	6563	-0.320	2056	286
[N II]	6583	-0.323	429	58.4
He I	6678	-0.336	43.7	5.5
[S II]	6716	-0.342	42.3	5.1
[S II]	6731	-0.344	44.1	5.3
He I	7065	-0.387	28.0	2.6
[Ar III]	7136	-0.396	129	11.2
C II	7236	-0.409	12.9:	1.0:
He I	7281	-0.414	12.1	0.94
[O II]	7320	-0.419	10.3:	0.78:
[O II]	7330	-0.420	7.2:	0.54:
[Ar III]	7751	-0.467	33.8	1.9
[Cl IV]	8046	-0.497	2.0:	0.1:
P16	8502	-0.540	25:	0.9:
P15	8545	-0.542	16:	0.6:
P14	8599	-0.547	13:	0.4:
P13	8665	-0.553	29:	0.9:
P12	8750	-0.560	29:	0.9:
P11	8863	-0.569	35:	1.0:
P10	9015	-0.581	20:	0.6:
[S III]	9069	-0.585	787	21.3
P $\zeta$	9229	-0.597	94.6	2.4

$E(B - V)$ , using the nebular Balmer decrement from our three independent WiFeS spectra, where the intrinsic line strengths from Hummer & Storey (1987) and the reddening law of Howarth (1983) were used. We independently determined the extinction by comparing the integrated 1.4 GHz and H $\alpha$  fluxes from § 3.2 (see, e.g. Bojičić et al. 2011b). We also utilised the P $\zeta$ /H $\alpha$  decrement, again adopting the line strengths from Hummer & Storey (1987).

Following Crowther et al. (2006a), interstellar  $K_S$ -band extinctions were also estimated from the observed  $J - K_s$  and  $H - K_s$  colours of the ionizing star, derived from Table 7. To estimate the intrinsic colours, we take the average of the values for the weak-lined WN 3–4 and WN 5–6 subgroups from Crowther et al. (2006a), i.e.  $(J - K_s)_0 = +0.04$  and  $(H - K_s)_0 = +0.07$ . Using the recipe of Crowther et al. (2006a), we calculate  $K_S$ -band extinctions of  $A_{K_s}^{J-K_s} = 0.78$  and  $A_{K_s}^{H-K_s} = 0.84$ , respectively. Adopting the mean value,  $A_{K_s} = 0.81$ , and using the relation between  $A_{K_s}$  and  $E(B - V)$  from Indebetouw et al. (2005), we derive  $E(B - V) = 2.3 \pm 0.3$ , in fair agreement with the other determinations. An independent, albeit lower accuracy estimate is derived from the equivalent width (2.6 $\text{\AA}$ ) of the  $\lambda$ 6284 diffuse interstellar band (DIB) in the red (the only one measurable), and applying the relation of Friedman et al. (2011). Finally, we re-evaluated the estimate of  $A_V = 5.7$  mag from Wachter et al. (2010) by fitting the overall SED of the star, excluding the uncertain IRAC [8.0]-mag value, to deter-

<sup>6</sup> MIR false-colour imaging is also a powerful diagnostic indicator for classification purposes (e.g. Cohen et al. 2007, 2011; Parker et al. 2012).

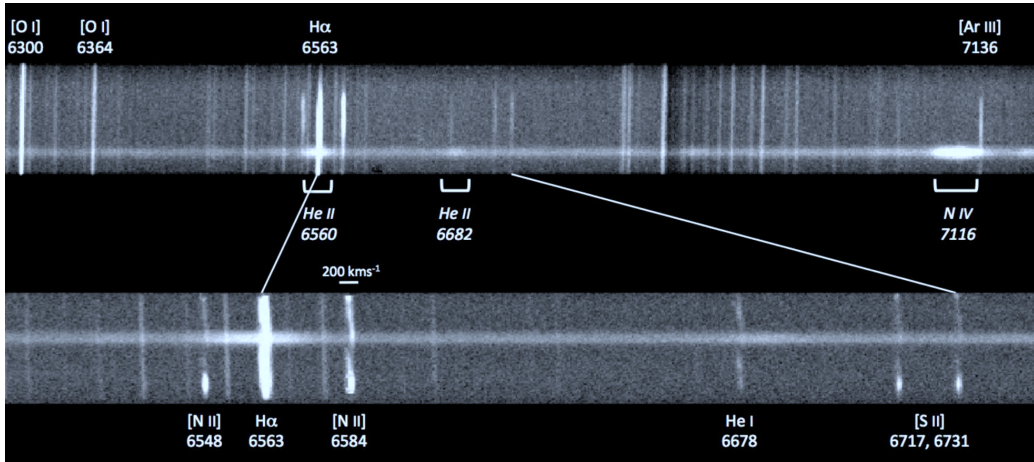


**Figure 4.** Individual image slices of our low-resolution ( $R = 3000$ ; top panel) and medium-resolution ( $R = 7000$ ; bottom panel) WiFeS red spectra showing the broad features from the CSPN, and line-splitting of the nebular lines due to expansion.

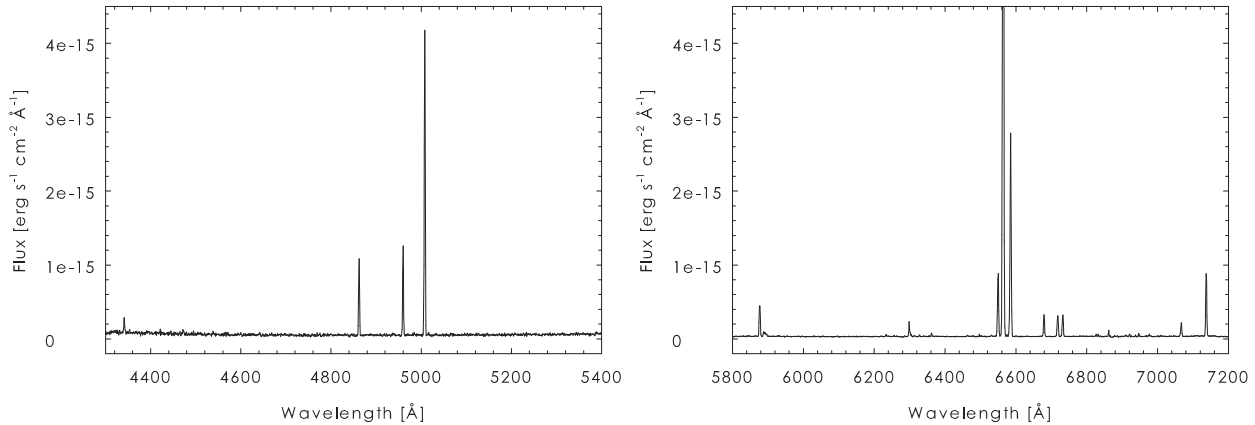


**Figure 5.** Extracts of the integrated blue (left) and red spectra of Abell 48, obtained from the high S/N WiFeS observation from 2012. Note that the  $H\alpha$  line is truncated in the right panel. The observed  $[N II]/H\alpha$  ratio is 0.28.

mine  $E(B - V) = 1.90 \pm 0.10$  (see § 4.4). We adopt an averaged reddening,  $E(B - V) = 1.90 \pm 0.10$  ( $c_{H\beta} = 2.75 \pm 0.15$ ) hereafter. This value can also be compared with the estimate of  $E(B - V) = 2.1$  ( $c_{H\beta} = 3.0$ ) from DePew et al. (2011), based on the nebular Balmer decrement from a shallow MSSSO 2.3-m spectrum, while TK13 determined  $E(B - V) = 2.10$  from a SED fit, and  $E(B - V) = 2.15$  from the Balmer decrement method.

### 3.3.2 Plasma Diagnostics

We estimated the nebular density of Abell 48 to be  $n_e = 700 \text{ cm}^{-3}$  from the observed ratio of the  $[S II]$  doublet. The  $[N II] \lambda 5755$  line is barely detected giving an uncertain value of the electron temperature, while the far red  $[S III]$  lines were used to estimate  $T_e = 7000 \text{ K}$ , and another low quality estimate comes from the ratio of the auroral to nebular  $[O II]$  lines. Two further estimates come from the relative strengths of the He I lines (Zhang et al. 2005). Despite the larger uncertainties of some of the fainter diagnostic lines, the independent estimates of the electron temperature are in

**Table 4.** A summary of the various reddening determinations for Abell 48 which are all in good agreement.

Method	$E(B - V)$
Stellar SED	$1.90 \pm 0.10$
Near-IR stellar colours	$2.3 \pm 0.3$
Radio/ $H\alpha$ flux	$1.77 \pm 0.15$
$H\alpha/H\beta$ decrement <sup>1</sup>	$2.2 \pm 0.2$
$H\alpha/H\beta$ decrement <sup>2</sup>	$1.92 \pm 0.1$
$H\alpha/H\beta$ decrement <sup>3</sup>	$1.85 \pm 0.1$
$P\zeta/H\alpha$ decrement <sup>1</sup>	$2.2 \pm 0.2$
$P\zeta/H\alpha$ decrement <sup>3</sup>	$1.8 \pm 0.2$
$\lambda 6284$ DIB	$1.9 \pm 0.5$
Adopted reddening	$1.90 \pm 0.15$

<sup>1</sup>From WiFeS spectrum 1; <sup>2</sup>WiFeS spectrum 2; <sup>3</sup>WiFeS spectrum 3.

good agreement, and we adopt an average value of 7500 K for the abundance analysis (§ 3.4). A summary is presented in Table 5.

**Table 5.** Summary of plasma diagnostics for Abell 48

Diagnostic	Value	Result
[S II] $\lambda 6717/\lambda 6731$	0.96	$N_e = 700 \text{ cm}^{-3}$
[N II] $(\lambda 6548 + \lambda 6584)/\lambda 5755$	195:	$T_e = 7600 \text{ K}$ :
[O II] $\lambda 3727/(\lambda 7320 + \lambda 7330)$	77:	$T_e = 6700 \text{ K}$ :
[S III] $(\lambda 9069 + \lambda 9532)/\lambda 6312$	198	$T_e = 6700 \text{ K}$ :
[O III] $(\lambda 4959 + \lambda 5007)/\lambda 4363$	>210:	$T_e < 9950 \text{ K}$
He I $\lambda 7281/\lambda 5876$	0.17	$T_e = 7300 \text{ K}$
He I $\lambda 7281/\lambda 6678$	0.053	$T_e = 7700 \text{ K}$
Gas temperature (adopted)	...	$T_e = 7500 \text{ K}$

### 3.3.3 Expansion Velocity

There do not appear to be any expansion velocity measurements for Abell 48 in the literature, so we used the WiFeS red-arm medium-resolution spectrum, taken in April 2010, to estimate the expansion velocity of the nebula from the gaussian profiles of the brightest nebular emission lines. The observed full-width at half-maximum (FWHM) for each line was determined using the *splot* function in IRAF, and the expansion velocity, corrected for instrumental resolution and thermal broadening, was calculated with the following expression (Giesekeing, Hippelein & Weinberger 1986):

$$v_{\text{exp}} = 0.5 (\text{FWHM}_{\text{obs}}^2 - \text{FWHM}_{\text{instr}}^2 - 8(\ln 2)k T_e/m)^{0.5} \quad (1)$$

where  $k$  is Boltzmann's Constant,  $T_e$  is the electron temperature taken from section 3.3,  $m$  is the atomic mass of the measured ion, and  $\text{FWHM}_{\text{instr}}$  is the instrumental FWHM determined from several night-sky lines. The HWHM is often taken to be equal to the expansion velocity (e.g. Weinberger 1989), but we instead use  $V_{10}$  (Medina et al. 2006) which is a better proxy for the expansion of the outer nebular rim (e.g. Schönberner et al. 2005). We derive  $V_{10} = 40 \text{ km s}^{-1}$ , which agrees with the average expansion velocity of sample of [WC] PNe,  $v_{\text{exp}}$  of  $36 \text{ km s}^{-1}$  (Peña, Medina & Stasińska 2003). From the same data-set we measure a heliocentric radial velocity of  $+36 \pm 3 \text{ km s}^{-1}$ , obtained using the IRAF package *emsaO*, which is lower than the velocity of  $+50 \pm 4 \text{ km s}^{-1}$  determined by TK13. Our measurement translates to a velocity relative to the local standard of rest of  $v_{\text{LSR}} = +49 \pm 3 \text{ km s}^{-1}$ .

This observed expansion velocity also falls in the range seen for the shells around late-WN (WNL) and luminous blue variable (LBV) stars (Nota et al. 1995; Chu 2003), but we point out that no point-symmetric, moderate-density ejecta shell is known to surround any massive WNE star. The earliest spectral type seen in a high-surface brightness coherent nebula is WN7b for PMR 5 (Frew et al., in preparation). Earlier WN stars possess increasingly one-sided, low-density shells, fragmented by Rayleigh-Taylor instabilities and having abundances diluted in part by swept-up gas from the diffuse ISM. An example is NGC 6888 (Gruendl et al. 2000; Fernández-Martín et al. 2012) around the WN6b(h) star WR 136.

## 3.4 Nebular Abundances

We derived ionic and total nebular abundances from our spectra using the EQUIB code (see Wesson, Stock & Scicluna 2012), after adopting the values of  $T_e$  and  $N_e$  given in Table 5. We determined the helium abundance from the measured intensities of the  $\lambda 5876$  and  $\lambda 6678$  He I recombination lines using the effective recombination coefficients from Hummer & Storey (1987). For the metallic ions, the abundances were derived from the observed line intensities of the strong collisionally-excited lines. We then derived the total abundances using the ionization correction factors (ICFs) de-

**Table 6.** Ionic abundances, adopted ionization correction factors and total abundances for Abell 48.

Line, $\lambda$ (Å)	Ion	Abundance
5876, 6678	He <sup>+</sup> /H <sup>+</sup>	0.129
	ICF(He)	1.00
	He/H	0.129
6548, 6584	N <sup>+</sup> /H <sup>+</sup>	2.21(−5)
	ICF(N)	2.75
	N/H	6.07(−5)
3727, 7325	O <sup>+2</sup> /H <sup>+</sup>	1.76(−4)
4957, 5007	O <sup>+2</sup> /H <sup>+</sup>	3.13(−4)
	ICF(O)	1.00
	O/H	4.89(−4)
3869	Ne <sup>+2</sup> /H <sup>+</sup>	1.10(−4)
	ICF(Ne)	1.57
	Ne/H	1.73(−4)
6717, 6731	S <sup>+</sup> /H <sup>+</sup>	5.51(−7)
6312, 9069	S <sup>+2</sup> /H <sup>+</sup>	1.15(−5)
	ICF(S)	1.10
	S/H	1.33(−5)
7136	Ar <sup>+2</sup> /H <sup>+</sup>	2.10(−6)
	ICF(Ar)	1.57
	Ar/H	3.30(−6)

rived from the expressions given in Kingsburgh & Barlow (1994). Note that the oxygen abundance has a larger uncertainty, as the nebular  $\lambda 3727$  [O II] doublet has an uncertain flux due to the high extinction. Furthermore, the neon abundance is only an indicative estimate, owing to the poor S/N ratio of the  $\lambda 3869$  [Ne III] line. The abundances and adopted ICFs are presented in Table 6. We note that TK13 derived a significantly higher electron temperature, and therefore a lower oxygen abundance than we do. Referring to the spectrum reproduced in their Figure 8, we see no sign of the [O III]  $\lambda 4363$  line, nor the neighbouring He I  $\lambda 4471$  line, which is predicted to be stronger by our photoionization model. Therefore we prefer our own upper limit for the [O III] electron temperature, and place more reliance in our nebular abundances.

Our analysis shows that Abell 48 has no significant enrichment of nitrogen ( $N/O \approx 0.12$ ) and does not belong to Peimbert's Type I class (Peimbert 1978; Peimbert & Torres-Peimbert 1983), for which we adopt Kingsburgh & Barlow's (1994) definition of  $N/O > 0.8$ . In fact, the nebular abundances are approximately solar, a point to which we return below. Here we differ from the conclusions of TK13, who find slightly subsolar abundances for Abell 48. We attribute this discrepancy to the higher electron temperature they adopt. We do not detect the [O III]  $\lambda 4363$  line which sets an upper limit on the electron temperature of  $\sim 10 \text{ kK}$ , and the mean of several independent diagnostics suggests a lower temperature of  $7500 \text{ K}$  (see Table 5), and hence a higher derived oxygen abundance. We will revisit the nebular abundances in § 5.2, § 6 and § 7.

## 4 THE CENTRAL STAR

### 4.1 Photometry

The CSPN is obvious on SuperCOSMOS  $B_J$ ,  $R_F$ ,  $I_N$ , and  $H\alpha$  images (Hambly et al. 2001; Parker et al. 2005), as well as 2MASS, UKIDSS and GLIMPSE images (Skrutskie et al. 2006; Lawrence et al. 2007; Benjamin et al. 2003). We summarise the available literature photometry in Table 7, along with new  $UBVI$  magnitudes measured by us. In order to correct the observed magnitudes and

**Table 7.** Summary of photometric measurements for the [WN4-5] central star of Abell 48. The third column gives the dereddened magnitudes.

Waveband	m	m <sub>0</sub>	Source
<i>U</i>	19.8 ± 0.2	10.6	This work
<i>B</i>	19.48 ± 0.02	11.7	This work
<i>V</i>	17.80 ± 0.01	11.9	This work
<i>V</i>	17.72 ± 0.25	11.8	YB6
<i>I</i>	15.50 ± 0.05	12.0	DENIS
<i>I<sub>c</sub></i>	15.14 ± 0.05	11.7	This work
<i>J</i>	13.54 ± 0.09	11.8	DENIS
<i>J</i>	13.508 ± 0.027	11.7	2MASS
<i>J</i>	13.440 ± 0.002	11.7	UKIDSS
<i>H</i>	12.834 ± 0.028	11.7	2MASS
<i>H</i>	12.823 ± 0.001	11.7	UKIDSS
<i>K<sub>s</sub></i>	12.302 ± 0.11	11.6	DENIS
<i>K<sub>s</sub></i>	12.325 ± 0.027	11.6	2MASS
<i>K<sub>s</sub></i>	12.281 ± 0.002	11.6	UKIDSS
[3.6]	11.69 ± 0.06	11.3	GLIMPSE
[4.5]	11.25 ± 0.10	11.0	GLIMPSE
[5.8]	11.06 ± 0.09	10.8	GLIMPSE
[8.0]	11.04 ± 0.16	10.8	GLIMPSE

References for photometry: 2MASS (Skrutskie et al. 2006); DENIS (Epchtein et al. 1994); GLIMPSE (Benjamin et al. 2003); UKIDSS (Lawrence et al. 2007); YB6 (Zacharias et al. 1994).

colours for reddening, a colour excess of  $E(B - V) = 1.90$  mag is adopted from § 3.3.1. The visual absorption is then  $A_v = 5.9$  mag using the reddening law of Howarth (1983).

No time series photometry of the CSPN is available, so information on any short-period variability is lacking. However *J* and *K<sub>s</sub>* magnitudes are available from three different epoch surveys, DENIS, 2MASS and UKIDSS (Epchtein et al. 1994; Skrutskie et al. 2006; Lawrence et al. 2007) and all agree within the uncertainties, so we can tentatively say the star is not a large amplitude variable, unlike the ionizing star of the LMC planetary N 66 (McKibben Nail & Shapley 1955), which is likely to host an interacting binary system (Hamann et al. 2003).

## 4.2 Spectroscopy

Spectroscopic classifications of the central star of Abell 48 were undertaken by Wachter et al. (2010) and DePew et al. (2011). Wachter et al. (2010) classified the central star as a WN6 according to the classification scheme developed by Conti, Massey & Vreux (1990). The previous shallow MSSSO 2.3m spectrum presented in DePew et al. (2011) showed a broad feature at  $\lambda 7116\text{\AA}$  in the red, but a large section of the spectrum between  $5050\text{\AA}$  and  $6300\text{\AA}$  was not observed, so it was unclear whether this was a [WN] or [WN/C] star. In our deeper spectra, we again find a strong feature centred around  $\lambda 7116\text{\AA}$ , attributed to the complex of N IV lines between  $\lambda 7103\text{\AA}$  and  $\lambda 7129\text{\AA}$ . The He II  $\lambda 6560$  line appears as a broad (FWHM  $\sim 25\text{\AA}$ ) feature from which the nebular H $\alpha$  line protrudes (the nebular lines are over-subtracted in the Palomar data). The He II  $\lambda 4686$  and  $\lambda 5412$  lines are prominent and a broad C IV  $\lambda \lambda 5801, 12$  doublet is also present, as is typical of the WN class.

We measured the stellar emission lines from all of our spectra using the `sp1ot` function in IRAF. Table 8 presents the identifications, the line equivalent widths (in  $\text{\AA}$ ), and the line widths (FWHM in  $\text{km s}^{-1}$ ) of the principal lines that were clearly detected. The typical uncertainties are 10–15% (no less than  $\pm 1\text{\AA}$  for the weak lines) and  $\pm 50 \text{ km s}^{-1}$  respectively, based on repeat measurements. The numerical criteria we used to classify the star are

**Table 8.** Principal emission lines found in the CSPN of Abell 48. The line equivalent widths and uncertainties are in  $\text{\AA}$ .

Species	$\lambda$ ( $\text{\AA}$ )	$-W_{\lambda}^a$ ( $\text{\AA}$ )	$-W_{\lambda}^b$ ( $\text{\AA}$ )	FWHM ( $\text{km s}^{-1}$ )
N IV	3480	...	45 ± 10	1300:
N IV	3748	...	3.0 ± 1.0	...
N IV	4058	...	23 ± 3	830
He II + N III	4100	...	29 ± 4	1060
He II + N III	4200	...	15 ± 2	800
He II	4339	...	11.5 ± 2.0	800
N III	4379	...	6.0 ± 1.0	...
N III	4518	...	12 ± 2.5	...
He II	4542	n.m.	16 ± 4	1200
N V	4604	n.m.	22.5 ± 3.0	560
N V	4620	n.m.	19.5 ± 3.0	600
N III	4634-40	...	12 ± 3	...
He II	4686	...	160 ± 20	1170
He II	4860	...	21.5 ± 4.5	1120
N III	4905	...	2.0 ± 1.0	...
N V	4944	n.m.	10.0 ± 3.0	...
N IV	5202	5.4 ± 2.0	5.0 ± 1.4	...
He II	5411	23 ± 4	34 ± 6	900
C IV	5806	...	15.2 ± 3.0	1300:
He I	5876	3.8 ± 2.0	n.m.	...
He II	6118	4.0 ± 1.4	2.2 ± 1.0	...
He II	6311	8.0 ± 2.0	5.4 ± 1.6	...
N IV	6382	3.8 ± 2.0	6.8 ± 2.0	800
He II	6406	7.1 ± 1.0	7.9 ± 1.0	...
He II	6527	4.3 ± 1.0	6.6 ± 1.0	...
He II	6560	130 ± 30	n.m.	1020
He I + He II	6683	...	...	blend
He II	6891	11.4 ± 1.0	10.4 ± 1.0	750
N IV	7116	160 ± 20	130 ± 10	1300
He II	7178	16.7 ± 3.2	...	...
He II + N IV	7590	n.m.	9.8 ± 2.0	450:
He II	8237	40.3 ± 5.3	31.1 ± 3.0	850
He II	9225	7.9 ± 1.8	...	700

<sup>a</sup> Second WiFeS spectrum; <sup>b</sup> Hale spectrum; n.m. = detected but not measured.

summarised in Table 9. Besides the high S/N Palomar spectrum, we also made use of our low-resolution WiFeS stellar spectrum, which extends to  $\sim 9500\text{\AA}$ , but very few classification schemes use the far-red / NIR wavelength region. As part of another project, we downloaded all the red spectra of the Galactic WN stars presented by Hamann, Koesterke & Wessolowski (1995), and measured the equivalent width of the  $\lambda 8237$  He II line for each star, if available. We tabulated the He II/He I ratios and spectral type from Smith, Shara & Moffat (1996) for each and found, as expected, a tight relation between the two quantities. This suggests a spectral class of [WN4] for the CSPN of Abell 48. In summary, the N IV  $\lambda 4057$  and N V  $\lambda \lambda 4604, 20$  lines being much stronger than the N III  $\lambda 4634, 40$  blend, with relatively weak C IV, we revisited the classification and now find an earlier type than [WN6] (c.f. Wachter et al. 2010), after primarily following the criteria of Smith et al. (1996). By giving most weight to the ratio of the equivalent widths of the He II  $\lambda 5411$  and He I  $\lambda 5876$  lines, our adopted classification is [WN4–5], while TK13 estimated a spectral class of [WN5].

We further note that there is no obvious indication of an oscillating Pickering decrement (e.g. Smith et al. 1996), showing that the star is hydrogen deficient. To quantitatively estimate the hydrogen fraction, we use the ‘Pickering index’ defined by Smith et al.

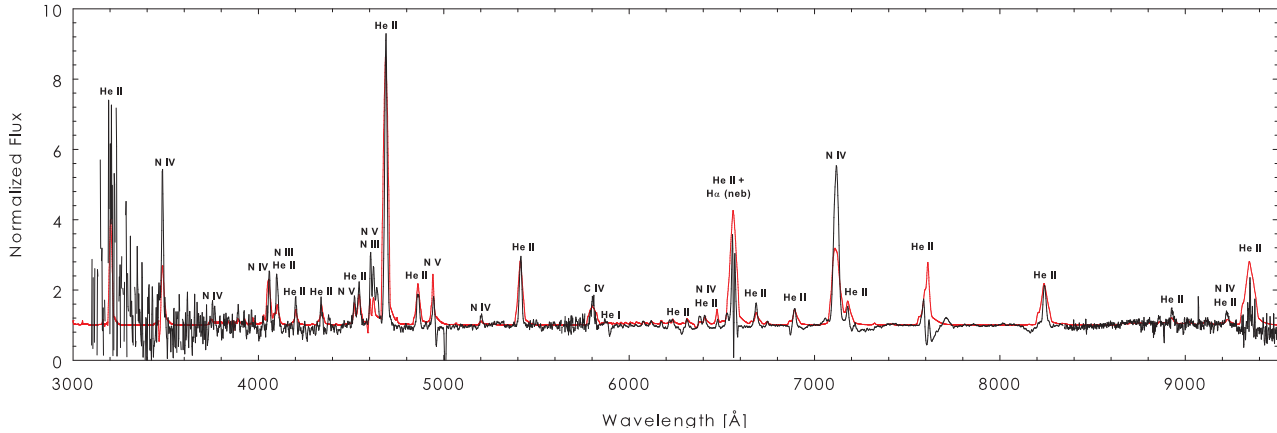


**Figure 6.** Normalized spectrum (black line) of the CSPN, spliced from our WiFeS and Palomar data. Note the presence of the N v  $\lambda\lambda 4604, 4620$  lines and the very prominent He II  $\lambda 4686$  and N IV  $\lambda 7116$  features in the spectrum. Overplotted is an updated model 10-13 (red line) from the Potsdam Wolf-Rayet (PoWR) grid, (provided by H. Todt), which fits the relative strengths of the He lines well. The relatively poor fit to the nitrogen lines suggests the default nitrogen abundance is too low. A colour version of this figure is available in the online journal.

**Table 9.** Classification of the central star, after Smith et al. (1996). The second column is the ratio of the measured equivalent widths.

Criterion	Ratio	Classification
$W_{\lambda 5411}/W_{\lambda 5876}$	9.5	WN4
$W_{\lambda 8237}/W_{\lambda 5876}$	7.8	WN4
$P_{5411}/P_{5876}$	2.6	WN5
$P_{4604}/P_{4640}$	1.6	WN5
$P_{4057}/P_{4604-40}$	0.8	WN4
$P_{5808}/P_{5876}$	1.6	WN5
$P_{5808}/P_{5411}$	0.6	WN4-5
Adopted	...	[WN4-5]

(1996; cf. Oliveira, Steiner & Cieslinski 2003):

$$\frac{N(\text{H}^+)}{N(\text{He}^{++})} = \frac{W(\lambda 4859 + \lambda 4861)}{[W(\lambda 4541) \times W(\lambda 5411)]^{0.5}} - 1 \quad (2)$$

Formally, we obtain the unphysical value of  $-0.1$ , which we reset to zero, on the basis of the observed uncertainties of the equivalent widths. In practice, we adopt a working upper limit for the hydrogen abundance of  $\sim 10\%$  based on the observed S/N ratio of the lines. Overall the spectrum is similar to a Population I WN4o star (Vreux, Dennefeld & Andrillat 1983; Smith et al. 1996), but as we show in Section 5, the properties of the surrounding nebula unambiguously show that we are dealing with low-mass CSPN.

### 4.3 Model Atmosphere Analysis

To begin the analysis, we downloaded the synthetic spectra appropriate for WNE model atmospheres from the Potsdam Wolf-Rayet (PoWR) database<sup>7</sup> (Hamann & Gräfener 2004) to compare with our data. These spectra are determined from the PoWR model atmospheres, described in Gräfener, Koesterke & Hamann (2002) and Hamann & Gräfener (2003), which account for spherical expansion, non-LTE effects, and metal line blanketing. The PoWR model grid has two dimensions, the stellar temperature  $T_*$  and the “transformed radius,”  $R_t$  (Hamann & Koesterke 1998), which is a wind

density parameter, being a function of the mass-loss rate,  $\dot{M}$ , and the stellar radius,  $R_*$ . It is given by:

$$R_t = R_* \left[ \frac{v_\infty}{2500 \text{ km s}^{-1}} / \frac{\dot{M} \sqrt{D}}{10^{-4} M_\odot \text{ yr}^{-1}} \right]^{2/3} \quad (3)$$

where  $v_\infty$  is the terminal velocity of the wind and  $D$  is a wind clumping factor (or inverse of the filling factor). It has been previously noted that many parameters of massive WRs and [WR]s are similar (e.g. Crowther, Morris & Smith 2006b), a consequence of the scaling law for WR atmospheres first noted by Schmutz, Hamann & Wessolowski (1989). In other words, two atmospheres with the same temperature ( $T_*$ ) and transformed radius ( $R_t$ ) show very similar spectra regardless of  $L_*$ ,  $R_*$ ,  $\dot{M}$  and  $v_\infty$ .

The PoWR grid models are normalized to  $L/L_\odot = 2.0 \times 10^5$  which is appropriate for a massive WN star; consequently, the stellar flux of our CSPN is proportional to  $L_*$ , and  $R_*$  and  $\dot{M}$  are proportional to  $L_*^{1/2}$  and  $L_*^{3/4}$  respectively. We follow Hamann & Koesterke (1998) in assuming a wind clumping factor of  $D = 4$  ( $f = 0.25$ ), which is appropriate for WN stars. The stellar radius,  $R_*$ , is the inner boundary of the model atmosphere and corresponds by definition to a Rosseland optical depth of 20. The stellar effective temperature,  $T_*$ , is the effective temperature at  $R_*$ , and can be easily calculated from the Stefan-Boltzmann law:

$$L = 4\pi R_*^2 \sigma T_*^4 \quad (4)$$

For Abell 48, various line ratios using the N III, N IV and N V, and He I and He II lines, initially constrained the temperature to between 63 and 79 kK and  $\log(R_t/R_\odot)$  between 0.6 and 1.0. The absence of He II  $\lambda 4686$  emission in the surrounding nebula is due to the optically thick WR wind. Models with  $T_{\text{eff}} < 60 \text{ kK}$  show a He I  $\lambda 5876$  line much stronger than observed, while models with  $T_{\text{eff}} > 90 \text{ kK}$  are ruled out as these produce significant flux shortward of the He II ionization edge at  $228 \text{ \AA}$ , so He II emission should be clearly present in the surrounding nebula. The estimated temperature is in broad agreement with the temperature range of 60–90 kK found for massive WN4 stars by Hamann & Gräfener (2003).

The best-fit model has  $T_{\text{eff}} = 71 \text{ kK}$  and  $R_t = 6.3 R_\odot$  (model 10-13) and reproduces fairly well the relative equivalent widths of the helium lines. A new synthetic spectrum calculated from a re-

<sup>7</sup> <http://www.astro.physik.uni-potsdam.de/~wrh/PoWR/powrgrid.html>, model 10-13, which utilised updated atomic data was kindly

provided by H. Todt (2013, pers. comm.) The model parameters are  $T_{\text{eff}} = 71\text{kK}$  and  $\log R_t = 0.8$ , with the default abundances set to He:C:N:O = 0.98: 1E-4: 0.015: 0.0. The observed and synthetic spectra are plotted in Figure 4.2). However, the N III, N IV and N V line intensities are all weaker in the model, in particular the N V 4944 and N IV 7116 blends. This indicates that the default nitrogen abundance is too low. We have not convincingly detected any line due to oxygen, so we make no modification to the default model abundance. Our parameters are in excellent agreement with that derived by TK13 (see their Table 3), the main difference is that TK13 estimate a higher nitrogen abundance of 5 percent and a hydrogen abundance of 10 per cent, a result that does not disagree with our upper limit for this element. So it is now apparent that the photospheric nitrogen and hydrogen abundances differ considerably between Abell 48 and IC 4663, mimicking the range of H abundances seen in the O(He) stars (Reindl et al. 2013, and references therein).

The intrinsic luminosity of the star, and hence its distance, is not constrained from the model atmosphere analysis. Instead we adopt the distance of 1.6 kpc from § 5.3 in the discussion that follows, cf. TK13 who assumed a canonical post-AGB luminosity. We found the bolometric correction of the model atmosphere to be  $-5.4$  mag, which leads to an estimated luminosity of the star of  $\sim 5.5 \times 10^3 L_{\odot}$ . From our adopted value of the temperature  $T_{\star}$ , the stellar radius  $R_{\star}$  was calculated using equation 4 to be  $0.49 R_{\odot}$ . From the line widths presented in Table 8, we estimate a terminal wind velocity,  $v_{\infty}$  of  $1200 \text{ km s}^{-1}$ . Finally, we estimate the mass-loss rate,  $\dot{M}$ , which is proportional to  $L^{3/4}$  for a constant  $R_t$  (equation 3). We determine  $\log \dot{M} = -6.3 \pm 0.2 M_{\odot} \text{ yr}^{-1}$ .

#### 4.4 Stellar Spectral Energy Distribution

The stellar spectral energy distribution (SED) for the CSPN of Abell 48 is shown in Figure 7, along with the adopted PoWR synthetic spectrum. The model has been normalized to the ensemble of the dereddened values from Table 7, excluding the Johnson  $U$  and IRAC  $8.0 \mu\text{m}$  magnitudes, which are both uncertain. We applied the optical and IR extinction laws of Howarth (1983) and Indebetouw et al. (2005) respectively, using  $E(B - V) = 1.90$ .

There is no evidence from our spectra for any signature of a companion star, nor from the SED for any NIR excess due to a cooler companion (Douchin et al. 2012; De Marco et al. 2013), though in this case any limit is not strong. The [WN] star is relatively luminous and the NIR magnitudes include a non-negligible contribution from wind free-free emission. As a result, any companion later than  $\sim F0V$  would not be detected. The tentative absence of variability (§4.1) suggests the star does not have an irradiated companion (De Marco, Hillwig & Smith 2008; Miszalski et al. 2009; Hajduk, Zilstra & Gesicki 2010), so time-series spectroscopic analysis is probably the best way to determine if Abell 48 is a binary (Jorissen & Frankowski 2008). However, at orbital periods greater than a year or two, the expected velocity shifts of the emission lines would be likely too small to be detected against the stochastic variations of the stellar wind.

## 5 THE NATURE OF ABELL 48

As a precursor to any discussion on the evolutionary implications of the [WN] class, it is important to try to properly assess all the observational evidence for Abell 48 so that its status as a true PN or a circumstellar nebula around a massive star can be made clear. Circumstellar nebulae can be morphologically similar to PNe, and

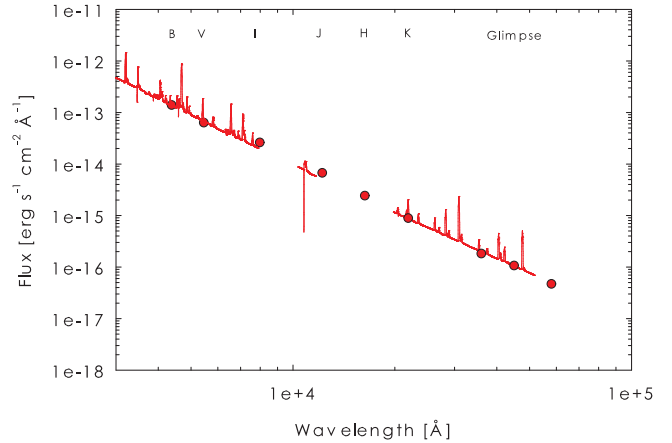


**Figure 7.** The SED of the central star of Abell 48. The red line shows the synthetic spectrum (PoWR model 10–13), with the photometric measurements dereddened with  $E(B - V) = 1.90$  plotted as red circles. A colour version of this figure is available in the online journal.

are found around several types of massive stars (Chu 2003; FP10; Mizuno et al. 2010; Wachter et al. 2010; Gvaramadze, Kniazev & Fabrika 2010; Bojičić et al. 2011a).

#### 5.1 Diagnostic plots

In Figure 8 we present the ‘SMB’ or  $\log F(\text{H}\alpha)/F[\text{N II}]$  versus  $\log F(\text{H}\alpha)/F[\text{S II}]$  diagnostic diagram of Sabbadin, Minello & Bianchini (1977), as extensively updated by Frew & Parker (2010, hereafter FP10), and further refined here (see also Sabin et al. 2013). Individual PNe are shown as small red dots and Galactic H II regions as small black squares. In the left panel the fields showing H II regions, SNRs and PNe are marked; note the considerable overlap between them. The blue triangles show the PNe with confirmed [WN] or [WN/C] stars, Abell 48, IC 4663, PB 8, along with NGC 6572, which has a candidate [WN/C] CSPN (Todt et al. 2012). These all plot squarely in the PN domain, while the orange diamond is N 66, the only PN in the LMC with a [WN] ionizing star. It shows substantial nitrogen enrichment compared to the mean LMC abundance.

The right panel shows the domain of LBV/WR ejecta, and the green triangles represent several ejecta nebulae based on literature data. These are all nitrogen enriched from CNO cycling, and mostly overplot the Type I PN region defined by FP10. Clearly, Abell 48 falls in the PN domain away from both Type I PNe and the CNO processed ejecta around LBV and WNL stars. This confirms our abundance analysis (§3.4 and §5.2) showing the nebula is not strongly nitrogen enriched, and unlikely to be produced by a massive star. While this part of the SMB diagram has extensive overlap between PNe and H II regions, Abell 48 is plainly not a H II region, as its morphology and MIR colours reveal. In particular the flux ratios,  $F_{12}/F_8 = 4.9$ ,  $F_{24}/F_8 = 5.5$ , and  $F_{70}/F_{12} = 9.2$  (see Table 2), strongly indicate a PN rather than a H II region (Anderson et al. 2012).

#### 5.2 Nebular Abundances

In Table 10, we summarise the elemental abundances for the four known PNe with confirmed [WN] or [WN]/[WC] central stars, compared with a selection of ring nebulae around massive stars.

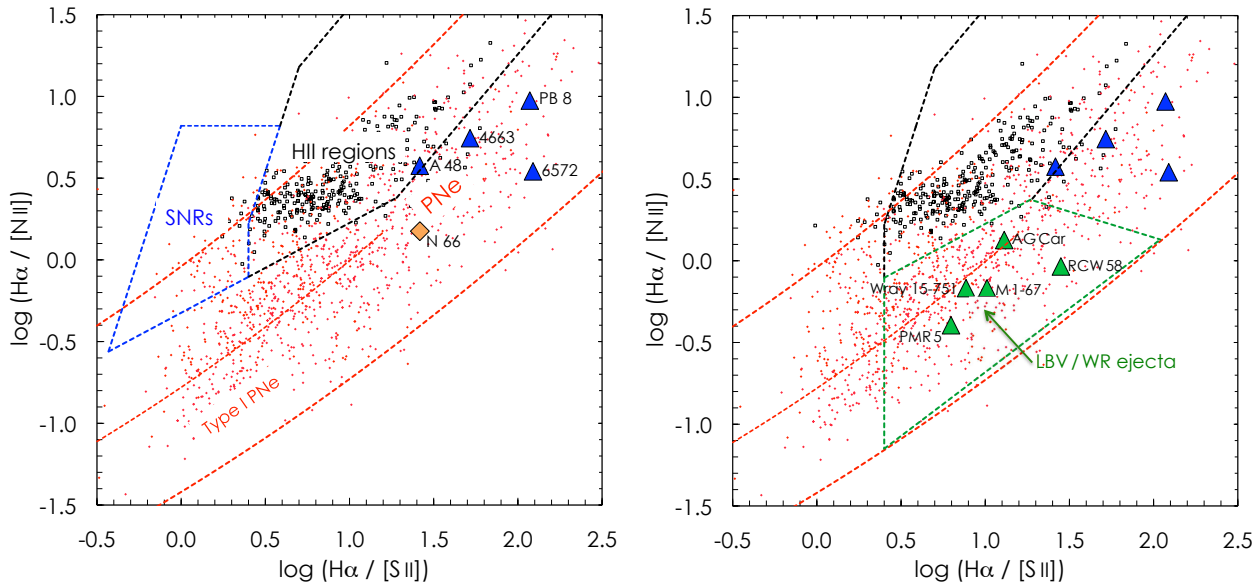


**Figure 8.** SMB diagnostic plots updated from FP10. Individual PNe are shown as small red dots and Galactic H II regions as small black squares. In the left panel the regions populated by HII regions, SNRs and PNe are marked; note the considerable overlap between them. The blue triangles show Abell 48, IC 4663, PB 8, and NGC 6572, which has a candidate [WN/C] CSPN (Todt et al. 2012). These all plot squarely in the PN domain, while the orange diamond is the LMC planetary N 66. In the right panel the domain of LBV/WR ejecta is plotted, and the green triangles plot a selection of ejecta nebulae. A colour version of this figure is available in the online journal.

As noted above, Abell 48 appears to have no significant nitrogen enrichment, and modest He enrichment, so it does not belong to Peimbert’s Type I class (Peimbert 1978; Kingsburgh & Barlow’s 1994). We use the nebular argon abundance as a metallicity indicator, as its abundance is predicted to be unaltered by nuclear processes in PN progenitor stars. We conclude that the progenitor of Abell 48 was slightly metal rich with  $[\text{Ar}/\text{H}] = +0.12$  dex, but owing to the uncertainty of the model-dependent ICF for argon (only one ionization stage is observed), Abell 48 is consistent with having a solar argon abundance. The metal abundances of PB 8 (Todt et al. 2010a) and IC 4663 (MC12) are similar, being approximately solar, or perhaps slightly more metal rich. We also note that the evolved PNe K 1-27 and LoTr 4, around O(He) stars, also show only modest helium enrichment, but the detailed CNO abundance pattern is difficult to determine for these very high excitation, optically thin PNe (Rauch, Koppen & Werner 1994, 1996).

Also recall that strongly enhanced nitrogen and helium abundances are expected, and seen, in the ejecta around massive LBV and WNL stars that are undiluted by swept-up ISM (Dufour 1989; Kwitter 1981, 1984; Esteban et al. 1992; Smith et al. 1994; Lamers et al. 2001; Stock, Barlow & Wesson 2011). LBV and WR ejecta also show evidence of oxygen depletion (e.g. Dufour 1989), as seen in Table 10, but the oxygen abundance of Abell 48 is very close to solar. The N/O mass ratio is high in LBV and WNL ejecta, ranging up to  $\sim 200$  for the ejecta around the peculiar WR-like star NaSt 1 (Crowther & Smith 1999), while the value for Abell 48 is only 0.12, rather typical of non-Type I PNe (Kingsburgh & Barlow 1994).

### 5.3 Distance

As the distance is critical to the interpretation of Abell 48, we revisit this problem here. Wachter et al. (2010) utilized the IRAC and 2MASS photometry to determine a large distance of 16.5 kpc on the assumption of Population I status, placing it on the far side of

the Galactic disk beyond the bulge. To refine this estimate, we adopt the absolute magnitude calibration for WR stars from Crowther et al. (2006a). We average the  $K_s$ -band absolute magnitudes for the WN 3-4 and WN 5-6 subgroups from their Table A1 to adopt  $M_{K_s} = -3.8 \pm 0.7$ . Our dereddened  $K_s$  magnitude from Table 7 leads to a distance modulus of 15.4 mag, or a distance of  $12.0_{-3.3}^{+4.6}$  kpc, again placing it on the far side of the Galactic bar. The luminosity follows from the distance, reddening and bolometric correction (§4.3), and is  $L \approx 3.4 \times 10^5 L_{\odot}$ .

The asymptotic reddening in this direction from Schlafly & Finkbeiner (2011, who updated Schlegel et al. 1998) is  $E(B - V) = 10.0$  mag ( $A_V \simeq 31$  mag), compared to our adopted  $E(B - V)$  of 1.90 ( $A_V = 5.9$ ). Even though the asymptotic extinction is not very reliable in this case, there should be at least 15–20 mag of visual extinction if the star is really at or on the far side of the end of the Galactic bar. Hence the discrepancy of such a large distance with a relatively low reddening is difficult to explain if we are dealing with a massive star, a point made by Wachter et al. (2010). The available data strongly suggest the star is closer and that it is likely to be the central star of a PN. Our argument is illustrated in Figure 9, which shows the asymptotic reddening as a function of Galactic longitude (Schlafly & Finkbeiner 2011), plotted for two latitudes,  $b = 0$  (the mid-plane) and  $b = 0.45$  (the latitude of Abell 48). It is clear that the reddening to Abell 48 is a small fraction of the total reddening in this direction. The sightline passes close to the intersection of the Galactic Long Bar with the Scutum-Centaurus arm where several major star-forming complexes and massive clusters occur, visible only in the IR (Negueruela et al. 2010, 2012, and references therein). The heavy interstellar extinction precludes the *optical detection* of any nebula beyond  $D = 6$  kpc on this sightline.

We can also determine a kinematic distance if we assume the nebula partakes of circular motion around the Galactic centre, albeit with an associated distance ambiguity in this direction. Since Abell 48 shows no obvious sign of an ISM interaction, any pecu-

**Table 10.** Elemental abundances, normalized to  $\log(H) = 12.0$ , for the three confirmed Galactic PNe with [WN] or [WN/WC] central stars, and N 66 in the LMC, compared to a sample of ejecta-dominated nebulae around massive stars. The reference sources are given in the footnotes to the table. For comparison, we also list the average abundances for Type I and non-Type I PNe, the abundances of the Orion nebula, and the solar abundances from Asplund et al. (2009).

Name	SpT	He	N	O	Ne	S	Ar	N/O	[O/H]	[Ar/H]	Reference
Abell 48	[WN4–5]	11.11	7.78	8.69	8.2:	7.12	6.52	0.12	+0.00	+0.12	This work
IC 4663	[WN3]	11.11	8.26	8.70	8.11	7.02	6.43	0.36	+0.01	+0.03	MC12
PB 8	[WN6/C7]	11.09	8.21	8.76	8.13	7.31	6.64	0.28	+0.07	+0.24	GR09
LMC-N66	[WN4.5]	11.04	7.97	8.37	7.93	6.68	6.11	0.40	−0.32	−0.29	P95,T03,B04
NaSt 1	pec	...	8.87	6.56	7.89	6.94	6.43	200	−2.13	+0.03	CS99
$\eta$ Car	LBV	11.26	9.04	7.29:	7.98	(7.1)	(6.4)	56:	−1.4 :	(0.0)	DG97
AG Car	WN11h	...	8.22	7.52	...	>6.7	...	5.0	−1.17	...	SS97
Hen 3-519	WN11h	...	8.21	7.57	...	...	...	4.4	−1.12	...	S97
Wray 15-751	WN11h	...	8.6:	<8.4	...	...	...	>1.6	<−0.3	...	GL98
M 1-67	WN8h	11.18	8.45	7.98	...	6.96	...	3.0	−0.71	...	EV91
NGC 6888	WN6b(h)	11.27	8.41	8.14	...	7.18	...	1.9	−0.55	...	EV92
NGC 6164-5	O6.5f?p	>11.11	8.13	8.25	7.5:	7.1	>6.3	0.76	−0.44	>−0.1	DP88
Type I PN	...	11.11	8.72	8.65	8.09	6.91	6.42	1.17	−0.04	+0.02	KB94
non-Type I PN	...	11.05	8.14	8.69	8.10	6.91	6.38	0.28	+0.00	−0.02	KB94
Solar	...	10.93	7.83	8.69	7.93	7.12	6.40	0.14	0.00	0.00	AG09
Orion	...	10.99	7.78	8.67	8.05	7.08	6.49	0.13	+0.04	+0.22	D84, EP04
LMC	...	10.99	7.14	8.35	7.61	6.70	6.29	0.06	−0.32	−0.11	RD92

References: AG09 – Asplund et al. (2009); B04 - Bernard-Salas et al. (2004); CS99 – Crowther & Smith (1999); D84 – Dufour (1984); DP88 – Dufour et al. (1988); DG97 – Dufour et al. (1997); EP04 – Esteban et al. (2004); EV91 – Esteban et al. (1991); EV92 – Esteban & Vilchez (1992); GL98 – Garcia-Lario et al. (1998); GR09 – García-Rojas et al. (2009); KB94 – Kingsburgh & Barlow (1994); MC12 – Miszalski et al. (2012b); P95 – Peña et al. (1995); RD92 – Russell & Dopita (1992); S97 – Stroud (1997); SS97 – Smith et al. (1997); T03 – Tsamis et al. (2003).

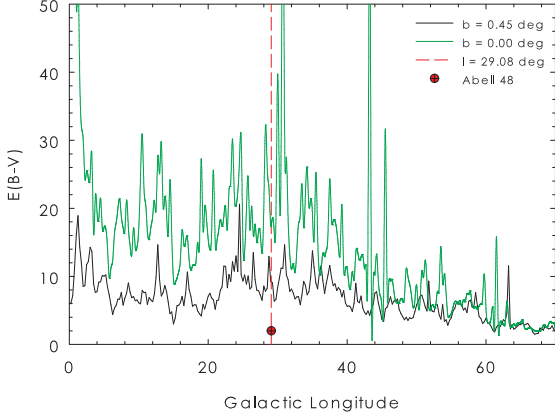


**Figure 9.** The distribution of reddening with Galactic longitude (Schlafly & Finkbeiner 2011), plotted for two Galactic latitudes,  $b = 0$  (the mid-plane) and  $b = 0.45$  (the latitude of Abell 48). It can be clearly seen that the reddening to Abell 48 is a small fraction of the asymptotic reddening on that sightline, precluding any location for the nebula beyond the Galactic bar.

liar velocity is not large (cf. TK13). The systemic velocity,  $v_{lsr} = +49 \pm 3 \text{ km s}^{-1}$  (see §3.3.3) indicates a kinematic distance of either  $3.2 \pm 1.8 \text{ kpc}$  or  $12 \pm 2.0 \text{ kpc}$ , after assuming the IAU standard circular velocity at the solar circle of  $220 \text{ km s}^{-1}$ . The uncertainties on the distances are dominated by the velocity dispersions of the respective stellar populations. However, owing to the heavy extinction along this sightline, we strongly favour the closer distance.

On the assumption that Abell 48 is a normal planetary, we can calculate a distance using its observed properties. Using the  $H\alpha$  surface brightness – radius ( $S_{H\alpha-r}$ ) relation (Frew & Parker 2006; Frew et al. 2006, 2013c; Frew 2008), and adopting our angular diameter, reddening, and total  $H\alpha$  flux, we derive a distance of  $1.6 \pm 0.4 \text{ kpc}$ , updated from a preliminary estimate of  $2.0 \text{ kpc}$  (Bojičić et

al. 2013). Adopting this distance, the Galactic latitude,  $b$  of  $0.45^\circ$  leads to a  $|z|$  height of  $\sim 13 \text{ pc}$ , indicating that Abell 48 is almost on the Galactic mid-plane.

#### 5.4 Derived Nebular Properties

In this section we use the surrounding ionized nebula as a diagnostic tool to investigate whether the central star is a massive WN star or a post-AGB star of much lower luminosity. To do this we use the angular diameter, integrated  $H\alpha$  flux and the reddening to determine the nebular size and ionized mass, at distances appropriate for the two contrasting interpretations of the central star. In particular, the ionized mass is an important reality check of our distance, and therefore all of the nebular and stellar properties that depend on it. We calculated the ionized mass of the nebula following Hua & Kwok (1999), who derived the expression:

$$M_{ion} = 0.032 (\epsilon/0.6)^{0.5} \theta^{1.5} D^{2.5} F_0(H\alpha)^{0.5} M_\odot \quad (5)$$

where  $\theta$  is in arcmin,  $D$  is in kpc,  $F_0(H\alpha)$  is the dereddened flux in units of  $10^{-12} \text{ erg cm}^{-2} \text{ s}^{-1}$ , and  $\epsilon$  is the filling factor.

We estimate the mass for two different distance estimates, applicable to a PN central star and a massive WN star. At  $1.6 \text{ kpc}$ , the estimated ionized mass has a sensible value of  $M_{ion} \simeq 0.3\sqrt{\epsilon} M_\odot$ . This is consistent with other PNe, which typically have ionized masses ranging from  $5 \times 10^{-3}$  to  $3 M_\odot$  (FP10). For the massive star interpretation, we adopt a distance of  $12.0 \text{ kpc}$ . This leads to a nebular mass,  $M_{ion} \simeq 50\sqrt{\epsilon} M_\odot$ , which even allowing for a very low filling factor, can be ruled out. The nebula has a mean radius of  $0.16 \text{ pc}$  if the distance is  $1.6 \text{ kpc}$ , typical of a middle-aged PN. Using  $v_{exp} = 40 \text{ km s}^{-1}$  (§3.3.3), the dynamical age is  $\sim 3900$  years with an uncertainty dominated by the distance error (or 30%). A summary of parameters for the two contrasting interpretations is presented in Table 11. In summary, based on the overall body of evidence (see FP10), Abell 48 is clearly a planetary nebula and not a Population I ring nebula on the far side of the bulge.

**Table 11.** An abbreviated comparison of quantities, taken from sections 4–6, and a qualitative assessment of the likelihood that Abell 48 a PN or a Population I ring nebula respectively.

Parameter	PN	Ring nebula
Distance (kpc)	1.6	12.0
Radius (pc)	0.16	1.2
$M_{\text{ion}}/M_{\odot}$	$0.3\sqrt{\epsilon}$	$50\sqrt{\epsilon}$
Nebular morphology	✓	✗
Nebular ionized mass	✓	✗
Extinction–distance relation	✓	✗
Diagnostic line ratios	✓	✗
Nebular abundances	✓	✗
Expansion velocity	✓	✓
Nebular MIR colours	✓	✗
MIR/radio flux ratio	✓	✓
$ z $ distance from plane	✓	✓

## 6 A SURVEY OF [WN] CENTRAL STARS

The [WR] CSPNe descend from intermediate-mass progenitors, exhibiting a different subclass distribution to the WR stars. Among the 100+ Galactic [WR] CSPNe, almost all are either [WC] or [WO] stars (Crowther et al. 1998; DePew et al. 2011). The existence of a [WN] class has long been controversial (Hamann et al. 2003; Werner & Herwig 2006; FP10; Todt et al. 2010b; MC12). WN stars are found in the nebulae M 1-67 and DuRe 1 (Bertola 1964; Duerbeck & Reipurth 1990), both formerly classified as PNe, but are now known to be WN8 stars surrounded by CNO-processed ejecta (Cohen & Barlow 1975; Crawford & Barlow 1991a,b; Marchenko et al. 2010; Fernández-Martín et al. 2013).

Since then, the central stars of LMC-N66 (Peña 1995; Peña et al. 2004; Hamann et al. 2003, 2005) and PMR 5 (Morgan, Parker & Cohen 2003) were classified as possible [WN] stars, and a new [WN/WC] class (Todt et al. 2010a,b, 2012) was introduced to accommodate the spectroscopic characteristics of the ionizing star of PB 8. More recently, DePew et al. (2011) identified the CSPN of Abell 48 as either a [WN] or [WN/C] star (cf. Wachter et al. 2010) and the CSPN of IC 4663 was found to be a bona fide [WN3] star (MC12). The CSPN of IC 4663 is rather weak-lined and is likely to be close to its evolutionary transformation into a O(He) star (MC12). The surface chemistry is dominated by helium, with a modest amount of nitrogen (about a quarter that of Abell 48), no hydrogen, and a relatively low oxygen abundance.

LMC-N66 (SMP 83) is an unusual, high-excitation, quadrupolar nebula (Peña & Ruiz 1988; Dopita et al. 1993; Peña et al. 1997) in the Large Magellanic Cloud. It is ostensibly a PN, as it has a diameter and ionized mass within PN limits, though with a high expansion velocity (Dopita et al. 1985). The central star is both photo-metrically variable (McKibben Nail & Shapley 1955) with an amplitude of  $\sim 1$  mag, and spectroscopically variable (Torres-Peimbert et al. 1993; Peña 2002; Peña et al. 2008); Peña (1995) classified it as a [WN4–5] star. A good review of this object was provided by Hamann et al. (2003), who investigated several interpretations for it. All things considered, they concluded that a binary evolution channel is most likely, either a massive star which has lost its surrounding hydrogen through a common-envelope interaction with a less massive companion, or it represents a white dwarf (WD) that is accreting mass from a companion and undergoes quasi-stable nuclear burning. If this is the case, it may be related to the supersoft X-ray (SSX) sources (Greiner 2000) and their kin, the V Sge stars (Diaz & Steiner 1995; Steiner & Diaz 1998). The latter scenario would suggest that N66 is a potential Type Ia SN progenitor.

**Table 12.** Properties of Abell 48, IC 4663, and PB 8, and their CSPNe. We include the results for Abell 48 from TK13 as a comparison. Data for IC 4663 and PB 8 are from MC12 and Todt et al. (2010a) respectively, unless otherwise indicated.

Object	Abell 48 <sup>b</sup>	Abell 48 <sup>c</sup>	IC 4663	PB 8
Distance (kpc)	1.6	1.9	3.5	4.2
Radius (pc)	0.16	0.2	0.13	0.07 <sup>d</sup>
Nebular age (yr)	3900	6500	4900	3200 <sup>d</sup>
$\log S(\text{H}\alpha)^a$	−2.2	...	−2.2 <sup>d</sup>	−1.5 <sup>d</sup>
$M_{5007}$	−0.7	...	−1.9 <sup>d</sup>	−0.7 <sup>d</sup>
Spectral type	[WN4–5]	[WN5]	[WN3]	[WN6/C7]
$T_*$ (kK)	71	70	140	52
$L_*$ ( $L_{\odot}$ )	5500	6000	4000	6000
$v_{\infty}$ (km s <sup>−1</sup> )	1200	1000	1900	1000
$\log R_t$ ( $R_{\odot}$ )	0.8	0.85	1.13	1.43
$R_*$ ( $R_{\odot}$ )	0.49	0.54	0.11	0.96
$\log \dot{M}$ ( $M_{\odot}\text{yr}^{-1}$ )	$-6.3^{+0.3}_{-0.2}$	$-6.4 \pm 0.2$	$-7.7^{+0.6}_{-0.2}$	$-7.1^{+0.2}_{-0.1}$

<sup>a</sup>Reddening-corrected surface brightness (erg cm<sup>−2</sup> s<sup>−1</sup> sr<sup>−1</sup>);

<sup>b</sup>This work; <sup>c</sup>TK13; <sup>d</sup>Frew et al. (in preparation).

We note that the unusual quasi-Wolf-Rayet star HD 45166, which is a close binary (Steiner & Oliveira 2005; Groh, Oliveira & Steiner 2008) exhibits a WN5 spectrum, and transient nitrogen-rich WR winds are also seen in symbiotic novae (Thackeray & Webster 1974; Nussbaumer 1996) and are probably due to phases of quasi-stable nuclear burning on the WDs in these binary systems.

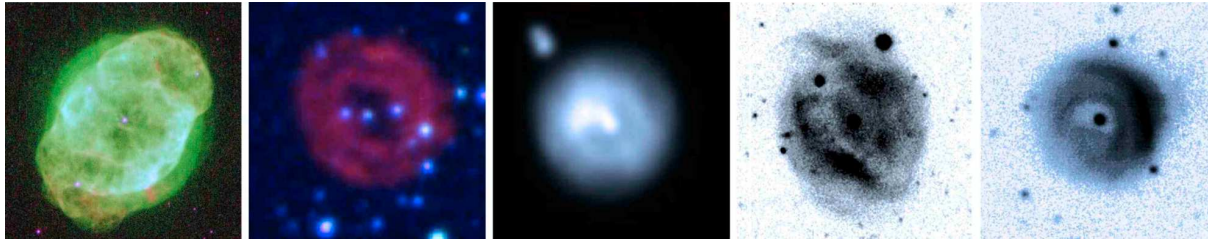
Recently, the PN status of PMR 5 was questioned by Werner & Herwig (2006) and Todt et al (2010b). We have now re-classified this star from a deep WiFeS spectrum, and revise the classification to WN7b. We have also found that the surrounding ejecta is composed of strongly CNO-processed material. A high-resolution VLT H $\alpha$  + [N II] image showing a flocculent appearance was presented by MC12, showing morphological similarities to RCW 58 (Chu 1982; Stock & Barlow 2010) and PCG 11 (Cohen, Parker & Green 2005) which surround WN8h stars. A fuller account on PMR 5 will be published separately (Frew et al., in preparation).

Figure 10 presents a montage of the three confirmed Galactic PNe with [WN] and [WN/WC] stars, along with the two PNe surrounding O(He) stars, K 1-27 and LoTr 4, included as a morphological comparison. Table 12 compares the fundamental properties of Abell 48, IC 4663, and PB 8, and their CSPNe. All three PNe are middle-aged, with PB 8 being the smallest object with the highest H $\alpha$  surface brightness. These values are corrected for reddening, and are derived from the dimensions given in Tylenda et al. (2003). None of these PNe are particularly luminous, as their absolute  $\lambda 5007$  magnitudes are 2.6 to 3.8 magnitudes below the bright cut-off of the PN luminosity function (e.g. Ciardullo 2010). Furthermore, the fact that none of these nebulae are particularly young leads to the question: what are their progenitors?

## 7 SIBLINGS, PROGENITORS AND PROGENY

### 7.1 Siblings

The surface composition of the CSPN of Abell 48 (see Table 13) is similar to the products of hydrogen-shell burning, i.e. mainly helium with a moderate amount of nitrogen (see also MC12 and TK13), though the nitrogen surface abundance in the CSPN of Abell 48 is to our knowledge, the highest known in a post-AGB star. If the carbon and oxygen in the progenitor was fully converted to



**Figure 10.** A montage of the bona fide Galactic PNe with [WN] and [WN/WC] CSPNe, plus the PNe K 1-27 and LoTr 4 which surround O(He) stars (not to the same scale). Left to right are IC 4663, Abell 48, PB 8, K 1-27 and LoTr 4. Abell 48 is a  $H\alpha/SR/B_J$  false-colour composite, while the images of IC 4663, PB 8, K 1-27, LoTr 4 are taken from Hajian et al. (2007), Schwarz et al. (1992), Rauch et al. (1998) and Rauch et al. (1996) respectively. A colour version of this figure is available in the online journal.

nitrogen via efficient CNO cycling, then the progenitor must have had a substantially supersolar metallicity to explain the high observed nitrogen abundance, but this appears marginally inconsistent with the nebular abundances (§ 3.4). Otherwise, additional mixing and mass-loss processes have occurred. The existence of [WN/WC] and [WN] CSPNe implies that there are additional post-AGB evolutionary pathways leading to hydrogen deficiency than previously assumed (De Marco 2002; Werner & Herwig 2006; Werner 2012; Frew & Parker 2011, 2012), but at present the full diversity of abundances is not explained by stellar evolution theory.

Recall there are three primary post-AGB evolutionary scenarios which are thought to produce H-deficient stars, all of which involve a thermal pulse (Iben et al. 1983; Herwig 2001; Werner & Herwig 2006), but which differ from each other in the point in the stellar evolutionary track when the thermal pulse occurs. These are the AGB Final Thermal Pulse (AFTP), the Late Thermal Pulse (LTP), and the Very Late Thermal Pulse (VLTP) scenarios (see Werner & Herwig 2006, for a review), and the photospheric nitrogen abundance of the star in question is an important diagnostic of the stage during which the final pulse occurs (Werner 2012).

Similar surface abundances to the [WN] stars are also seen in a few, but not all, of the low-gravity, ‘luminous’ He-sdO stars (e.g. Husfeld et al. 1989; Jeffery 2008; Napiwotzki 2008; Heber 2009), none of which are convincingly associated with PNe (Méndez et al. 1988). These stars (Heber 2009), alternatively termed sdO(He) stars (Rauch et al. 1998), lie in the same region of the Hertzsprung-Russell (HR) diagram<sup>8</sup> as Abell 48. Indeed, a close analogue is the sdO(He) star LSE 263 (Husfeld et al. 1989) but which is not surrounded by any detectable PN. It is feasible that some luminous He-sdO stars are just the lower-mass analogues of the [WN] stars. If this is correct, the smaller  $L/M$  ratios in the He-sdOs explains the absence of any strong wind features, as they are less proximate to the Eddington Limit, and their lower masses explain the absence of any detectable PNe, owing to the long post-AGB timescales of these ‘lazy’ remnants (Schönberner 1983; Méndez et al. 1988; Blöcker 1995). Table 13 gives a summary of the photospheric abundances seen in a range of H-normal and H-deficient post-AGB stars, grouped on the basis of their compositions. The top group contains H-normal stars, and the next two groups are helium-rich, greater than about 80% by mass, but differing in the ratios of N to C + O. The following two groups have substantial residual hydrogen, again

separated by their N to C ratios, while the lower three groups are those with PG1159 abundances ( $He \sim C > O$ ), hydrogen-rich or ‘hybrid’ PG1159 compositions (Napiwotzki & Schönberner 1991), and H/He-deficient compositions, respectively. It is likely that there are gradual transitions between the various groups, especially of the hydrogen and helium contents (e.g. Rauch & Kerber 2005), and that the divisions in Table 13 are somewhat arbitrary.

## 7.2 Progenitors and Progeny

Werner & Herwig (2006), Werner (2012) and MC12 have commented on the strong compositional and evolutionary links between the O(He) and [WN] stars, but the overall origin of this group of objects is currently being debated. Only four O(He) stars are known, two with surrounding nebulae (Rauch, Dreizler & Wolff 1998; Reindl et al. 2013). However, the two stars without observed PNe, HS 1522+6615 and HS 2209+8229, appear to be nitrogen poor (see Table 13) and may be evolutionary unrelated to the [WN] stars. Another example might be Abell 52 (Rauch & Kerber 2005), which has the  $N \vee \lambda, \lambda 4604, 20$  lines in emission, and has detectable hydrogen, with  $He/H \approx 4$  by mass. Other He-rich stars such as the naked sdO, KS 292 (Rauch et al. 1991), and its PN-shrouded analogue GJJC 1 in M 22 (Harrington & Paltoglou 1993) have rather more hydrogen, and moderate nitrogen and carbon abundances.

Rauch et al. (2008) suggested two possible evolutionary scenarios for the formation of the O(He) stars. They are either the offspring of the R CrB stars which are strongly H-deficient cool, variable supergiants, that may derive in turn from low-mass WD mergers (Clayton et al. 2007), or alternatively, they might be post early-AGB or post-RGB stars (Werner 2012). Wassermann et al. (2010) found the hot He-rich pre-WD KPD 0005+5106 to have a similar photospheric abundances to the R CrB (Clayton 1996; Asplund et al. 2000) and the extreme-helium (EHe) stars (Pandey et al. 2006; Pandey & Lambert 2011). Wassermann et al. (2010) also considered KPD 0005+5106 and the R CrB stars to be WD merger products which form a separate evolutionary post-AGB sequence.

On theoretical grounds, Saio & Jeffery (2002) concluded that a merger of a carbon-oxygen WD with a less-massive helium WD is a viable model for the formation of the ‘majority’ R CrB stars, which are compositionally dominated by helium, and have almost no hydrogen. More recently, Hema et al. (2012) found that the observed  $^{12}C/^{13}C$  isotopic ratios in the majority R CrB stars are also consistent with simple nucleosynthesis predictions for such a WD merger (see also Pandey & Lambert 2011; Jeffery, Karakas & Saio 2011). Yet, the observational evidence for R CrB itself is contradictory (Clayton et al. 2011), as the star is surrounded by a dusty nebula (or fossil PN?) suggesting a post-AGB origin. There is also

<sup>8</sup> The position of the luminous sdO stars in the HR diagram is consistent with post-AGB evolution, while the ‘compact’ sdOs are likely to derive from a post-extreme horizontal branch (EHB) route (Heber 2009). There are no known PNe around any post-EHB stars (Frew et al. 2010).

**Table 13.** Properties and elemental surface abundances (expressed as percentage mass fractions) of a selection of post-AGB stars and pre-WDs.

Name	SpT	$T_*$ (kK)	$\log g$ (cgs)	$X_H$	$X_{He}$	$X_C$	$X_N$	$X_O$	$X_{Ne}$	PN?	Reference
H-rich composition; $C + O > N$											
K 648	sdO	39	3.9	74	24	0.9	0.001	1.2	...	y	RH02
NGC 1535	O(H)	85	4.8	74	25	0.2	0.1	0.8	0.2	y	HB04a, HB11
Sh 2-216	DAO	95	6.9	95	4	0.1	0.1	0.2	...	y	RZ07
Lo 1	O(H)	120	6.7	69	28	0.2	0.1	2.5	0.2	y	HB04b
He-rich composition; $N \gg C + O$											
V652 Her	EHe-B	25	3.7	0.2	99	0.01	0.8	0.04	0.3	n	JH99
LSE 263	sdO(He)	70	4.9	<2	98	0.03	1.6	...	...	n	H89
Abell 48	[WN4-5]	71	4.9	10	85	0.3	5.0:	<0.6	...	y	TK13, this work
LoTr 4	O(He)	120	5.5	12	87	<0.07	0.7	<0.02	<0.1	y	R13
PG 1034+001	DO	120	6.7	<1.2	98	0.02	0.4	0.04	0.13	n <sup>†</sup>	MR12
K 1-27	O(He)	130	6.0	4.7	93	<0.06	1.3	<0.01	<0.5	y	R13
IC 4663	[WN3]	140	6.1	<2	>95	<0.1	0.8	0.05	0.2	y	MC12
He-rich composition; $N < C + O$											
R CrB	G0Iab:pe	6.8	0.5	0.001	97	1.4	0.3	1.2	...	(y)	AG00
BD +10° 2179	EHe-B	16	2.5	0.01	99	1.7	0.1	0.1	0.1	n	PL11
BD +37° 442	sdO(He)	48	4.0	<0.1	97	2.5	0.3	...	...	n	BH95, JH10
HS 2209+8229	O(He)	110	6.0	<0.6	99	<0.01	<0.1	0.1	<0.01	n	R13
HS 1522+6615	O(He)	130	5.9	0.8	98	1.0	<0.01	0.13	<0.03	n	R13
KPD 0005+5106	DO	200	6.7	<2.5	98	1.0	0.3	0.4	0.4	n	WW10
He $\geq$ H; $C \sim N$											
PB 8	[WN6/C7]	52	4.2	40	55	1.3	2.0	1.3	...	y	T10
KS 292	sdO	75	5.0	32	65	2.3	1.3	...	...	n	R91
He $\geq$ H; $N \gg C + O$											
NGC 2392	O6f	47	4.0	42	57	0.008	0.4	0.01	...	y	MU12, HB11
HD 49798	sdO5.5	47	4.3	19	78	<0.01	2.5	...	...	n	BP97
PG 1159 composition (He $\sim C + O$ )											
NGC 40	[WC8]	78	5.0	<2	43	51	...	6	...	y	MD07
Abell 58	[WC4]	95	...	...	54	40	...	5	...	y	CK06
NGC 6751	[WO4]	135	6.0	...	54	31	1.5	15	...	y	LK93, KH97
PG 1159-035	PG1159	140	7.0	<2	33	48	0.1	17	2	n	JR07
RX J2117.1+3412	PG1159	163	6.6	...	39	32	...	22	...	y	CA07
Lo 4	[WO]-PG1159	170	6.0	...	38	54	...	6	2	y	WRK10
Hybrid PG 1159 composition (He $\sim C > H, O$ )											
IRAS 21282+5050	[WC11]h	28	3.2	10	43	46	<0.5	1.0	...	y	WH06
Abell 43	PG1159h	105	5.6	24	56	19	0.02	0.2	...	y	RF11
HS 2324+3944	PG1159h	130	6.2	17	35	42	...	6	...	n	DW96
H- and He-deficient composition ( $C \sim O$ )											
H 1504+65	PG1159pec	200	8.0	...	<1	48	...	48	2	n	WR04

References: AG00 – Asplund et al. (2000); BH95 – Bauer & Husfeld (1995); BP97 – Bisscheroux et al. (1997); CA07 – Corsico et al. (2007); CK06 – Clayton et al. (2006); DW96 – Dreizler et al. (1996); H89 – Husfeld et al. (1989); HB04a, HB04b – Herald & Bianchi (2004a,b); HB11 – Herald & Bianchi (2011); JH99 – Jeffery, Hill & Heber (1999); JR07 – Jahn et al. (2007); KH97 – Koesterke & Hamann (1997); LK93 – Leuhenagen et al. (1993); MC12 – Miszalski et al. (2012b); MD07 – Marcolino et al. (2007); MR12 – Mahsereci et al. (2012); MU12 – Méndez et al. (2012); PL11 – Pandey & Lambert (2011); R91 – Rauch et al. (1991); R13 – Reindl et al. (2013); RF11 – Ringat et al. (2011); RH02 – Rauch et al. (2002); RW95 – Rauch & Werner (1995); RZ07 – Rauch et al. (2007); T10 – Todt et al. (2010a); TK13 – Todt et al. (2013); WH06 – Werner & Herwig (2006); WR04 – Werner et al. (2004); WW10 – Wasserman et al. (2010). Notes: <sup>†</sup> PG 1034+001 is the ionizing star of the “planetary nebula” Hewett 1, but this is probably just ionized ambient ISM (Chu et al. 2004; Madsen et al. 2006; Frew 2008).

a small group of RCB stars with some residual hydrogen and a peculiar abundance pattern, the ‘minority’ RCB stars, but their origin is also a mystery (Rao & Lambert 2008). As noted by TK13, the hydrogen abundance of Abell 48 is  $\sim 10\%$ . In this respect the CSPN of Abell 48 differs both from the [WN/C] ionizing star of PB 8, and the CSPN of IC 4663 (Todt et al. 2010a; MC12). An AFTP is unlikely to produce a star with an abundance pattern as seen in Abell 48, as hydrogen abundances are predicted to exceed 15%, the exact amount depending on the mass of the envelope at the time of the AGB final dredge-up. Moreover, a hybrid PG 1159 composition is expected, whereby the C (+O) abundance should greatly exceed the N abundance (Werner & Herwig 2006). An LTP scenario is also excluded, as this reduces the nitrogen abundance to only  $\sim 0.1\%$ , and the emission lines attributed to N IV and N V would be expected to be very weak in the optical (Werner et al. 2009). On the

other hand a VLTP model requires that the remaining hydrogen will be completely consumed, with surface abundances less than  $10^{-7}$  by mass, however, the observed CNO mass fractions of Abell 48 are not matched by this scenario. It is important to recall that the standard LTP scenario (Herwig 2001; Werner & Herwig 2006) cannot explain the helium-rich abundances seen in these stars.

### 7.3 Are Binary Channels Needed?

So how do the [WN] stars fit in to this framework? The observed surface abundances appear to require the substantial processing of initial carbon and oxygen to nitrogen, followed by removal of the H-rich envelope, possibly via mass transfer in an Algol-type binary system. Recall however, that the nebular abundances for Abell 48 and IC 4663 are close to solar (MC12; TK13; this work), so the ob-

served PNe are not simply the stripped atmospheres of these stars. Furthermore, with the exception of a few objects like V652 Her (Jahn et al. 2007), most EHe (and the R CrB) stars differ from the [WN] stars in having photospheric  $N < C$ , suggesting different evolutionary routes for the two groups. There appears to be a similar dichotomy amongst the O(He) stars, though firm conclusions will only come with a larger sample. Notwithstanding these caveats, a binary post-AGB (or even a post-RGB) evolutionary channel with mass exchange (Iben & Tutukov 1985), may be required to produce the [WN] stars, rather than an outright merger (cf. MC12). Guerrero et al. (2013) has suggested an analogous scenario for the formation of the quadrupolar PN, Kn 26 (Jacoby et al. 2010).

Recently, Herald & Bianchi (2011) found the unusual CSPN of the Eskimo nebula, NGC 2392, to show enhanced nitrogen and a deficiency of carbon and oxygen, but with substantial residual hydrogen. This had been earlier noted by Méndez (1991) and Pauldrach, Hoffmann & Méndez (2004). This abundance pattern suggests a second dredge-up may have occurred (e.g. Kingsburgh & Barlow 1994; Marigo et al. 2003), but this is expected only for a narrow range of initial mass, between 3–5  $M_{\odot}$ . However, other evidence suggests that the Eskimo CSPN is derived from a lower-mass progenitor (Pottasch, Bernard-Salas & Roellig 2008). Interestingly, Méndez et al. (2012) suggest that the abundance pattern is the result of truncated evolution due to a close binary interaction, and there is observational evidence (Pottasch et al. 2008; Danehkar et al. 2012) which suggests that its CSPN has an accreting companion, which is detected in hard X-rays (Kastner et al. 2012; Ruiz et al. 2013). So are the [WN] stars also the product of a binary scenario?

Alternatively, there may be other more exotic post-AGB channels worth considering. For example, Miller Bertolami et al. (2011) have suggested that diffusion-induced CNO-flashes in a cooling WD, the diffusion-induced nova (DIN) scenario, might apply to PB 8 and the peculiar variable CK Vul (Hajduk, van Hoof & Zijlstra 2013, and references therein). While the surface abundance of nitrogen is enhanced in the DIN scenario, we deem this to be unlikely for Abell 48, as the requirement of a low-metallicity WD progenitor does not appear to be met. Furthermore, the nebular ionized mass is typical of post-AGB ejected material, and such a significant mass ejection is not expected from a WD with a cooling age of  $10^6$  to  $10^7$  years (see Miller Bertolami et al. 2011).

Overall, a variety of evolutionary pathways for CSPN evolution is indicated, based on a review of the recent and current literature (e.g. Méndez 1991; Werner 1992; Rauch et al. 1998; Herwig 2001; Blöcker 2001; De Marco et al. 2002; Miller Bertolami & Althaus 2006; Werner & Herwig 2006; Todt et al. 2010a; Werner 2012; Quirion, Fontaine & Brassard 2012). Table 14 summarizes these pathways. The first column defines an initial condition for the evolutionary route, the second column gives the route in symbolic form, and the last column gives some candidate examples, primarily drawn from Table 13. On the basis of the data presented in Table 14, it seems that more theoretical work is required to explain post-AGB stars with an Abell 48-like abundance pattern, with or without residual surface hydrogen. It seems the last two proposed evolutionary pathways are the most viable alternatives, either a previously unknown post-AGB evolutionary route, perhaps a post-early AGB pathway, with mass exchange truncating the evolution, or a binary merger of two WDs.

## 8 CONCLUSIONS AND FUTURE WORK

On the basis of an extensive set of new and archival observations, we have undertaken a comprehensive analysis of the planetary nebula Abell 48 and its CSPN, first classified by Wachter et al. (2010) and DePew et al. (2011). Based on the presence of very strong N IV lines and moderately strong N V lines at  $\lambda\lambda 4604, 4620$  relative to N III  $\lambda\lambda 4634, 4640$ , we now classify it as [WN4–5] star with little or no hydrogen. We confirm Abell 48 as a bona fide PN after a detailed comparison of the properties of the nebula and its central star. If it was a massive star, the distance would be about 12 kpc, and the ionized mass of the nebula would be nearly  $\sim 50 M_{\odot}$ , which is much too high even for a Population I ejecta nebula. Moreover if it were located at or beyond the Galactic Bar, it would suffer much more extinction than observed, and would be optically invisible. We have estimated a new distance of 1.6 kpc, and an ionized mass of  $\sim 0.3 M_{\odot}$ , a value typical of other PNe. Our results are in substantive agreement with the independent study by TK13.

The relationships of the [WN] and [WN/C] stars to other post-AGB stars were also investigated, and we consider it likely that there are two separate channels producing He-rich stars, as distinct from the He- and C- dominated PG1159 stars (see Table 13 and Table 14 for examples). Population modelling should be useful in helping to unravel the origin of the [WN] and related objects. Unfortunately these stars are rare — only three or four Galactic [WN] and [WN/C] stars and four or five O(He) stars are presently known (Rauch et al. 1998, 2009; Reindl et al. 2012; MC12; TK13, and this work). The space density of the O(He) stars is expected to be higher than their [WN] progenitors, in a similar vein to the observed ratio of PG 1159 to [WC] stars in a volume-limited sample of PNe (refer to the data of Frew 2008). This is because the observed space densities are directly related to the time a star spends on the nuclear burning and WD cooling tracks respectively.

As noted by Frew & Parker (2011, 2012), the current sample of the so-called weak emission-line stars (WELS; Tylanda et al. 1993; Gesicki et al. 2006), a seemingly diverse group, may hold several more [WN] and [WN/C] stars awaiting identification on the basis of better spectra. Indeed, PB 8 was previously identified as a transitional object (Méndez 1989; Parthasarathy et al. 1998) and IC 4663 as a ‘WELS’ (Weidmann & Gamen 2011), before their discovery as [WN] stars. In light of this, there are several more candidate [WN] or [WN/C] stars that we are following up, including PMR 1 (Morgan, Parker & Russeil 2001), PMR 3 (Parker & Morgan 2003), PMR 8 (Mabee 2004), PHR J1757-1649 (DePew et al. 2011) and Kn 15 (Kronberger et al. 2012). The CSPN of M 1-37 (Kudritzki et al. 1997; Hultzsch et al. 2007) is also a possible [WNL] candidate (see Figure 4 of Kudritzki et al. 1997).

Until more [WN] and O(He) stars are identified, and robust estimates of their space density, scale height and birth rate are established, it will be difficult to fully understand their relationships to other H-deficient stars, and consequently their formation mechanism(s). Time will tell if the [WN] CSPNe are the offspring of binary-induced mass exchange, a WD merger, or instead represent the progeny of a previously unknown single-star post-AGB evolutionary pathway. It is clear that much more work is still to be done.

## ACKNOWLEDGEMENTS

We thank the anonymous referee for comments that significantly improved this manuscript. D.J.F. thanks Macquarie University for a MQ Research Fellowship and I.S.B. is the recipient of an

**Table 14.** Potential evolutionary pathways for post-AGB stars.

Initial condition	Pathway	Examples
No final He flash	TP-AGB $\rightarrow$ O(H) $\rightarrow$ DAO $\rightarrow$ DA	NGC 1535, NGC 7293, Sh 2-216
AFTP	TP-AGB $\rightarrow$ Ofc/[WC] $\rightarrow$ PG1159h $\rightarrow$ DA	Abell 43, NGC 7094, Sh 2-68
LTP	post-AGB $\rightarrow$ AGB $\rightarrow$ [WC] $\rightarrow$ [WO] $\rightarrow$ PG1159 $\rightarrow$ DO $\rightarrow$ DB	NGC 40, PG1159-035, PG1520+525
Weak LTP?	post-AGB $\rightarrow$ AGB $\rightarrow$ [WN/C]h $\rightarrow$ DAO $\rightarrow$ DA	PB 8
VLTP	pre-WD $\rightarrow$ AGB $\rightarrow$ [WC] $\rightarrow$ [WO] $\rightarrow$ PG1159 $\rightarrow$ DO $\rightarrow$ DB	Sakurai's object, FG Sge
Mass transfer / stripping?	eAGB $\rightarrow$ He-sdO or [WN] $\rightarrow$ O(He) $\rightarrow$ DO $\rightarrow$ DB	Abell 48, LMC N66?
He-WD + CO-WD merger	R CrB $\rightarrow$ EHe $\rightarrow$ O(He) $\rightarrow$ DO $\rightarrow$ DB	R CrB, KPD 0005+5106?
High-mass progenitor	SAGB $\rightarrow$ PG1159pec/DO? $\rightarrow$ hot DQ $\rightarrow$ DQZ	H1504+65?

Australian Research Council Super Science Fellowship (project ID FS100100019). This research has made use of the SIMBAD database and the VizieR service, operated at CDS, Strasbourg, France, and used data from the AAO/UKST H $\alpha$  Survey, produced with the support of the Anglo-Australian Telescope Board and the UK Particle Physics and Astronomy Research Council (now the STFC). Q.A.P and M.S. acknowledge support from the Australian Astronomical Observatory.

## REFERENCES

- Abell G.O., 1955, *PASP*, 67, 258  
 Abell G.O., 1966, *ApJ*, 144, 259  
 Acker A., Ochsenbein F., Stenholm B., Tylenda R., Marcout J., Schohn C., 1992, *Strasbourg-ESO Catalogue of Galactic Planetary Nebulae*. ESO, Garching  
 Acker A., Neiner C., 2003, *A&A*, 403, 659  
 Ali A., Sabin L., Snaid S., Basurah H.M., 2012, *A&A*, 541, A98  
 Allamandola L. J., Tielens A.G.G.M., Barker J.R., 1989, *ApJS*, 71, 733  
 Anderson L.D., Zavagno A., Barlow M.J., Garca-Lario P., Noriega-Crespo A., 2012, *A&A*, 537, A1  
 Asplund M., Gustafsson B., Lambert D.L., Rao N.K., 2000, *A&A*, 353, 287  
 Asplund M., Grevesse N., Sauval A.J., Scott P., 2009, *ARA&A*, 47, 481  
 Bauer F., Husfeld D., 1995, *A&A*, 300, 481  
 Benjamin R.A. et al., 2003, *PASP*, 115, 953  
 Bernard-Salas J., Houck J.R., Morris P.W., Sloan G.C., Pottasch S.R., Barry D.J., 2004, *ApJS*, 154, 271  
 Bertola F., 1964, *PASP*, 76, 241  
 Bisscheroux B.C., Pols O.R., Kahabka P., Belloni T., van den Heuvel E.P.J., 1997, *A&A*, 317, 815  
 Blöcker T., 1995, *A&A*, 299, 755  
 Blöcker T., 2001, *Ap&SS*, 275, 1  
 Bojičić I.S., Parker Q.A., Filipović M.D., Frew D.J., 2011a, *MNRAS*, 412, 223  
 Bojičić I.S., Parker Q.A., Frew D.J., Vaughan A.E., Filipović M.D., Gunawardhana M.L.P., 2011b, *Astron. Nachr.*, 332, 697  
 Bojičić I.S., Frew D.J., Parker Q.A., Stupar M., Wachter S., DePew K., 2013, in Krzesinski J., Stachowski G., Moskalik P., eds, *ASP Conf. Ser.* 469, 18th European White Dwarf Workshop. Astron. Soc. Pac., San Francisco, p. 309  
 Carey S.J. et al., 2009, *PASP*, 121, 76  
 Chu Y.-H., 1982, *ApJ*, 254, 578  
 Chu Y.-H., 2003, in van der Hucht K., Herrero A., Esteban C., eds, *Proc. IAU Symp.* 212, *A Massive Star Odyssey: From Main Sequence to Supernova*. Astron. Soc. Pac., San Francisco, p. 585  
 Chu Y.-H., Gruendl R.A., Williams R.M., Gull T.R., Werner K., 2004, *AJ*, 128, 2357  
 Churchwell E. et al., 2009, *PASP*, 121, 213  
 Ciardullo R., 2010, *PASA*, 27, 149  
 Clayton G.C., 1996, *PASP*, 108, 225  
 Clayton G.C., Kerber F., Pirzkal N., De Marco O., Crowther P.A., Fedrow J.M., 2006, *ApJ*, 646, L69  
 Clayton G.C., Geballe T.R., Herwig F., Fryer C., Asplund M., 2007, *ApJ*, 662, 1220  
 Clayton G.C. et al., 2011, *ApJ*, 743, 44  
 Cohen M., Barlow M.J., 1975, *ApL*, 16, 165  
 Cohen M., Parker Q.A., Green A.J., 2005, *MNRAS*, 360, 1439  
 Cohen M. et al., 2007, *ApJ*, 669, 343  
 Cohen M., Parker Q.A., Green A.J., Miszalski B., Frew D.J., Murphy T., 2011, *MNRAS*, 413, 514  
 Condon J.J., Cotton W.D., Greisen E.W., Yin Q.F., Perley R.A., Taylor G.B., Broderick J.J., 1998, *AJ*, 115, 1693  
 Condon J.J., Kaplan D.L., 1998, *ApJS*, 117, 361  
 Conti P.S., Massey P., Vreux J.-M., 1990, *ApJ*, 354, 359  
 Córscico A.H., Althaus L.G., Miller Bertolami M.M., Werner K., 2007, *A&A*, 461, 1095  
 Crawford I.A., Barlow M.J., 1991a, *A&A*, 249, 518  
 Crawford I.A., Barlow M.J., 1991b, *A&A*, 251, L39  
 Crowther P.A., 2007, *ARA&A*, 45, 177  
 Crowther P.A., Smith L.J., 1999, *MNRAS*, 308, 82  
 Crowther P.A., De Marco O., Barlow M.J., 1998, *MNRAS*, 296, 367  
 Crowther P.A., Hadfield L.J., Clark J.S., Negueruela I., Vacca W.D., 2006a, *MNRAS*, 372, 1407  
 Crowther P.A., Morris P.W., Smith J.D., 2006b, *ApJ*, 636, 1033  
 Danehkar A., Frew D.J., Parker Q.A., De Marco O., 2012, in *Proc. IAU Symp.*, 282, *From Interacting Binaries to Exoplanets: Essential Modeling Tools*. CUP, Cambridge, p. 470  
 De Marco O., 2002, *Ap&SS*, 279, 157  
 De Marco O., Clayton G.C., Herwig F., Pollacco D.L., Clark J.S., Kilkenny D., 2002, *AJ*, 123, 3387  
 De Marco O., Hillwig T.C., Smith A.J., 2008, *AJ*, 136, 323  
 De Marco O., Passy J.-C., Frew D.J., Moe M.M., Jacoby G.H., 2013, *MNRAS*, 428, 2118  
 DePew K., 2011, PhD thesis, Macquarie University  
 DePew K., Parker Q.A., Miszalski B., De Marco O., Frew D.J., Acker A., Kovacevic A.V., Sharp R.G., 2011, *MNRAS*, 414, 2812  
 Diaz M.P., Steiner J.E., 1995, *AJ*, 110, 1816  
 Dopita M.A., Meatheringham S.J., 1990, *ApJ*, 357, 140  
 Dopita M.A., Ford H.C., Webster B.L., 1985, *ApJ*, 297, 593  
 Dopita M.A., Ford H.C., Bohlin R., Evans I.N., Meatheringham S.J., 1993, *ApJ*, 418, 804  
 Dopita M., Hart J., McGregor P., Oates P., Bloxham G., Jones D., 2007, *Ap&SS*, 310, 255  
 Dopita M.A. et al., 2010, *Ap&SS*, 327, 245  
 Douchin D. et al., 2012, in *Manchado A., Stanghellini L., Schönberner D., eds, Proc. IAU Symp.* 283, *Planetary Nebulae: An Eye to the Future*. Cambridge Univ. Press, Cambridge, p. 346  
 Duerbeck H.W., Reipurth B., 1990, *A&A*, 231, L11  
 Dufour R.J., 1984, *Proc. IAU Symp.*, 108, 353  
 Dufour R.J., 1989, *Rev. Mex. Astron. Astrofis.*, 18, 87  
 Dufour R.J., Parker R.A.R., Henize K.G., 1988, *ApJ*, 327, 859  
 Dufour R.J., Glover T.W., Hester J.J., Currie D.G., van Orsow D., Walter

- D.K., 1997, ASP Conf. Ser., 120, 255
- Dreizler S., Werner K., Heber U., Engels D., 1996, A&A, 309, 820
- Egan M.P. et al., 2003, Air Force Research Laboratory Technical Report AFRL-VS-TR-2003-1589
- Epchtein N. et al., 1994, Ap&SS, 217, 3
- Ercolano B., Barlow M.J., Storey P.J., Liu X.-W., 2003, MNRAS, 340, 1136
- Ercolano B., Barlow M.J., Storey P.J., 2005, MNRAS, 362, 1038
- Esteban C., Vilchez J.M., 1992, ApJ, 390, 536
- Esteban C., Vilchez J.M., Manchado A., Smith L.J., 1991, A&A, 244, 205
- Esteban C., Vilchez J.M., Smith L.J., Clegg R.E.S., 1992, A&A, 259, 629
- Esteban C., Peimbert M., García-Rojas J., Ruiz M.T., Peimbert A., Rodríguez M., 2004, MNRAS, 355, 229
- Fernández-Martín A., Martín-Gordón D., Vilchez J.M., Pérez Montero E., Riera A., Sánchez S.F., 2012, A&A, 541, A119
- Fernández-Martín A., Vilchez J.M., Pérez Montero E., Candian A., Sánchez S.F., Martín-Gordón D., Riera A., 2013, A&A, 554, A104
- Frew D.J., 2008, PhD Thesis, Macquarie University
- Frew D.J., Parker Q.A., 2006, Proc. IAU Symp., 234, 49
- Frew D.J., Parker Q.A., 2010, PASA, 27, 129 (FP10)
- Frew D.J., Parker Q.A., 2011, in Zijlstra A.A., Lykou F., McDonald I., Lagadee E., eds, APN V Conf. Proc. Jodrell Bank Centre for Astrophysics, article 33
- Frew D.J., Parker Q.A., 2012, in Manchado A., Stanghellini L., Schönberner D., eds, Proc. IAU Symp. 283, Planetary Nebulae: An Eye to the Future. Cambridge Univ. Press, Cambridge, p. 192
- Frew D.J., Parker Q.A., Russeil D., 2006, MNRAS, 372, 1081
- Frew D.J., Madsen G.J., O'Toole S.J., Parker Q.A., 2010, PASA, 27, 203
- Frew D.J. et al., 2011, PASA, 28, 83
- Frew D.J., Bojičić I.S., Parker Q.A., 2012, in Manchado A., Stanghellini L., Schönberner D., eds, Proc. IAU Symp. 283, Planetary Nebulae: An Eye to the Future. Cambridge Univ. Press, Cambridge, p. 362
- Frew D.J., Bojičić I.S., Parker Q.A., 2013, MNRAS, 431, 2
- Frew D.J., Bojičić I.S., Parker Q.A., Pierce M.J., Gunawardhana M.L.P., Reid W.A., 2014a, MNRAS, in press (arXiv:1303.4555)
- Frew D.J., Parker Q.A., Bojičić I.S., 2014b, MNRAS, submitted
- Friedman S.D. et al., 2011, ApJ, 727, 33
- García-Lario P., Riera A., Manchado A., 1998, A&A, 334, 1007
- García-Rojas J., Peña M., Peimbert A., 2009, A&A, 496, 139
- Gaustad J.E., McCullough P.R., Rosing W., Van Buren D., 2001, PASP, 113, 1326
- Gesicki K. et al., 2006, A&A, 451, 925
- Gieseking F., Hippelein H., Weinberger R., 1986, A&A, 156, 101
- Gooch R., 1996, ASP Conf. Ser., 101, 80
- Gräfener G., Koesterke L., Hamann W.-R., 2002, A&A, 387, 244
- Greiner J., 2000, NewA, 5, 137
- Groh J.H., Oliveira A.S., Steiner J.E., 2008, A&A, 485, 245
- Gruendl R.A., Chu Y.-H., Dunne B.C., Points S.D., 2000, AJ, 120, 2670
- Guerrero M.A., Miranda L.F., Ramos-Larios G., Vázquez R., 2013, A&A, 551, A53
- Gvaramadze V.V., Kniazev A.Y., Fabrika S., 2010, MNRAS, 405, 1047
- Hajduk M., Zijlstra A.A., Gesicki K., 2010, MNRAS, 406, 626
- Hajduk M., van Hoof P.A.M., Zijlstra A.A., 2013, MNRAS, 432, 167
- Hajian A. et al., 2007, ApJS, 169, 289
- Hamann W.-R., Koesterke L., 1998, A&A, 333, 251
- Hamann W.-R., Gräfener G., 2003, A&A, 410, 993
- Hamann W.-R., Gräfener G., 2004, A&A, 427, 697,
- Hamann W.-R., Koesterke L., Wesołowski U., 1995, A&AS, 113, 459
- Hamann W.-R., Peña M., Gräfener G., Ruiz M.T., 2003, A&A, 409, 969
- Hamann W.-R., Peña M., Gräfener G., 2005, ASP Conf. Ser., 334, 345
- Hambly N.C. et al., 2001, MNRAS, 326, 1279
- Harrington J.P., Paltoglou G., 1993, ApJ, 411, L103
- Heber U., 2009, ARA&A, 47, 211
- Helfand D.J., Becker R.H., White R.L., Fallon A., Tuttle S., 2006, AJ, 131, 2525
- Hema B.P., Pandey G., Lambert D.L., 2012, ApJ, 747, 102
- Herald J.E., Bianchi L., 2004a, ApJ, 609, 378.
- Herald J.E., Bianchi L., 2004b, PASP, 116, 391
- Herald J.E., Bianchi L., 2011, MNRAS, 417, 2440
- Herwig F., 2001, Ap&SS, 275, 15
- Howarth I.D., 1983, MNRAS, 203, 301
- Hua C.T., Kwok S., 1999, A&AS, 138, 275
- Hultsch P.J.N., Puls J., Méndez R.H., Pauldrach A.W.A., Kudritzki R.-P., Hoffmann T.L., McCarthy J.K., 2007, A&A, 467, 1253
- Hummer D.G., Storey P.J., 1987, MNRAS, 224, 801
- Husfeld D., Butler K., Heber U., Drilling J.S., 1989, A&A, 222, 150
- Iben I. Jr., Tutukov A.V., 1985, ApJS, 58, 661
- Iben I. Jr., Kaler J.B., Truran J.W., Renzini A., 1983, ApJ, 264, 605
- Indebetouw R. et al., 2005, ApJ, 619, 931
- IPAC, 1986, IRAS Catalog of Point Sources, Version 2.0, Vizier online catalogue, II/125
- Ishihara D. et al., 2010, A&A, 514, A1
- Jacoby G.H. et al., 2010, PASA, 27, 156
- Jahn D., Rauch T., Reiff E., Werner K., Kruk J.W., Herwig F., 2007, A&A, 462, 281
- Jeffery C.S., 2008, in ASP Conf. Ser., 391, 3
- Jeffery C.S., Hill P.W., Heber U., 1999, A&A, 346, 491
- Jeffery C.S., Karakas A.I., Saio H., 2011, MNRAS, 414, 3599
- Jorissen A., Frankowski A., 2008, AIP Conf. Ser., 1057, 1
- Kastner J.H. et al., 2012, AJ, 144, 58
- Kimeswenger S. et al., 1998, A&A, 332, 300
- Kingsburgh R.L., Barlow M.J., 1994, MNRAS, 271, 257
- Koesterke L., Hamann W.-R., 1997, A&A, 320, 91
- Kohoutek L., 2001, A&A, 378, 843
- Kronberger M. et al., 2012, in Manchado A., Stanghellini L., Schönberner D., eds, Proc. IAU Symp. 283, Planetary Nebulae: An Eye to the Future. Cambridge Univ. Press, Cambridge, p. 414
- Kudritzki R.P., Méndez R.H., Puls J., McCarthy J.K., 1997, Proc. IAU Symp., 180, 64
- Kwitter K.B., 1981, ApJ, 245, 154
- Kwitter K.B., 1984, ApJ, 287, 840
- Lamers H.J.G.L.M., Nota A., Panagia N., Smith L.J., Langer N., 2001, ApJ, 551, 764
- Landolt A.U., 2009, AJ, 137, 4186
- Lawrence A. et al., 2007, MNRAS, 379, 1599
- Leuenhagen U., Koesterke L., Hamann W.-R., 1993, Acta Astr., 43, 329
- López J.A., Richer M.G., Garca-Díaz, M.T., Clark D.M., Meaburn J., Riesgo H., Steffen W., Lloyd M., 2012, RvMxAA., 48, 3
- Mabee A., 2004, BSc (Honours) Thesis, Macquarie University
- Madsen G.J., Frew D.J., Parker Q.A., Reynolds R.J., Haffner L.M., 2006, in Barlow M.J., Méndez R.H., eds, Proc. IAU Symp. 234, Planetary Nebulae in our Galaxy and Beyond. Cambridge Univ. Press, Cambridge, p. 455
- Mahserici M., Ringat E., Rauch T., Werner K., Kruk J.W., 2012, in Proc. IAU Symp. 283, Planetary Nebulae: An Eye to the Future. Cambridge Univ. Press, Cambridge, p. 426
- Marchenko S.V., Moffat A.F.J., Crowther P.A., 2010, ApJ, 724, L90
- Marcolino W.L.F., Hillier D.J., de Araujo F.X., Pereira C.B., 2007, ApJ, 654, 1068
- Marigo P., Bernard-Salas J., Pottasch S.R., Tielens A.G.G.M. Wesselius P.R., 2003, A&A, 409, 619
- McKibben Nail V., Shapley H., 1955, Proc. NAS, 41, 685
- Medina S., Peña M., Morisset C., Stasińska G., 2006, RMxAA, 42, 53
- Méndez R.H., 1989, Proc. IAU Symp., 131, 261
- Méndez R.H., 1991, Proc. IAU Symp., 145, 375
- Méndez R.H., Gathier R., Simon K.P., Kwitter K.B., 1988, A&A, 198, 287
- Méndez R.H., Urbaneja, M.A., Kudritzki, R.P., Prinja, R.K., 2012, in Proc. IAU Symp. 283, Planetary Nebulae: An Eye to the Future. Cambridge Univ. Press, Cambridge, p. 436
- Miller Bertolami M.M., Althaus L.G., 2006, A&A, 454, 845
- Miller Bertolami M.M., Althaus L.G., Olano C., Jiménez N., 2011, MNRAS, 415, 1396
- Miszalski B., Acker A., Parker Q.A., Moffat A.F.J., 2009, A&A, 496, 813
- Miszalski B., Boffin H.M.J., Frew D.J., Acker A., Köppen J., Moffat A.F.J., Parker Q.A., 2012a, MNRAS, 419, 39
- Miszalski B., Crowther P.A., De Marco O., Köppen J., Moffat A.F.J., Acker A., Hillwig T.C., 2012b, MNRAS, 423, 934 (MC12)

- Mizuno D.R., et al., 2010, *AJ*, 139, 1542
- Monet D.G. et al., 2003, *AJ*, 125, 984
- Morgan D.H., Parker Q.A., Russeil D., 2001, *MNRAS*, 322, 877
- Morgan D.H., Parker Q.A., Cohen M., 2003, *MNRAS* 346, 719
- Napiwotzki R., 2008, *ASP Conf. Ser.*, 391, 257
- Napiwotzki R., Schönberner D., 1991, *A&A*, 249, L16
- Neguera I., González-Fernández C., Marco A., Clark J.S., Martínez-Núñez S., 2010, *A&A*, 513, A74
- Neguera I., Marco A., González-Fernández C., Jiménez-Esteban F., Clark J.S., García M., Solano E., 2012, *A&A*, 547, A15
- Nieva M.-F., Przybilla N., 2012, *A&A*, 539, A143
- Nota A., Livio M., Clampin M., Schulte-Ladbeck R., 1995, *ApJ*, 448, 788
- Nussbaumer H., 1996, *Ap&SS*, 238, 125
- O'Dell C.R., Ferland G.J., Henney W.J., Peimbert M., 2013, *AJ*, 145, 92
- Oliveira A.S., Steiner J.E., Cieslinski D., 2003, *MNRAS*, 346, 963
- Paladini R., Burigana C., Davies R.D., Maino D., Bersanelli M., Cappellini B., Platania P., Smoot G., 2003, *A&A*, 397, 213
- Pandey G., Lambert D.L., 2011, *ApJ*, 727, 122
- Pandey G., Lambert D.L., Jeffery C.S., Rao N.K., 2006, *ApJ*, 638, 454
- Parker Q.A., Morgan D.H., 2003, *MNRAS*, 341, 961
- Parker Q.A. et al., 2005, *MNRAS*, 362, 689
- Parker Q.A. et al., 2012, *MNRAS*, 427, 3016
- Parthasarathy M., Acker A., Stenholm B., 1998, *A&A*, 329, L9
- Pauldrach A.W.A., Hoffmann T.L., Méndez R.H., 2004, *A&A*, 419, 1111
- Peimbert M., 1978, in Terzian Y., ed., *Proc. IAU Symp. 76, Planetary nebulae*. D. Reidel, Dordrecht, p. 215
- Peimbert M., Torres-Peimbert S., 1983, in Flower D. R., ed., *Proc. IAU Symp. 103, Planetary nebulae*. D. Reidel, Dordrecht, p. 233
- Peña M., 1995, *Rev. Mex. Astron. Astrofis. Conf. Ser.*, 3, 215
- Peña M., 2002, *Rev. Mex. Astron. Astrofis. Conf. Ser.*, 12, 148
- Peña M., Ruiz M.T., 1988, *Rev. Mex. Astron. Astrofis.*, 16, 55
- Peña M., Peimbert M., Torres-Peimbert S., Ruiz M.T., Maza J., 1995, *ApJ*, 441, 343
- Peña M., Hamann W.-R., Koesterke L., Maza J., Méndez R.H., Peimbert M., Ruiz M.T., Torres-Peimbert S., 1997, *ApJ*, 491, 233
- Peña M., Medina S., Stasińska G., 2003, *Rev. Mex. Astron. Astrofis. Conf. Ser.*, 15, 38
- Peña M., Peimbert A., Hamann W.-R., Ruiz M.T., Peimbert M., 2004, *ASP Conf. Ser.*, 313, 131
- Peña M., Ruiz M.T., Rojo P., Torres-Peimbert S., Hamann, W.-R., 2008, *ApJ*, 680, L109
- Perek L., Kohoutek L., 1967, *Catalogue of Galactic Planetary Nebulae*. Prague: Publication House, Czechoslovak Academy of Sciences
- Phillips J.P., Marquez-Lugo R.A., 2011, *MNRAS*, 410, 2257
- Pierce M.J., Frew D.J., Parker Q.A., Köppen J., 2004, *PASA*, 21, 334
- Pottasch S.R., Bernard-Salas J., Roellig T.L., 2008, *A&A*, 481, 393
- Purcell C.R. et al., 2013, *ApJS*, 205, 1
- Quirion P.-O., Fontaine G., Brassard P., 2012, *ApJ*, 755, 128
- Rao N.K., Lambert D.L., 2008, *MNRAS*, 384, 477
- Rauch T., Kerber F., 2005, *ASP Conf. Ser.*, 334, 329
- Rauch T., Werner K., 1995, *Lecture Notes in Physics*, 443, 186
- Rauch T., Dreizler S., Wolff B., 1998, *A&A*, 338, 651
- Rauch T., Köppen J., Werner K., 1994, *A&A*, 286, 543
- Rauch T., Köppen J., Werner K., 1996, *A&A*, 310, 613
- Rauch T., Heber U., Hunger K., Werner K., Neckel T., 1991, *A&A*, 241, 457
- Rauch T., Heber U., Werner K., 2002, *A&A*, 381, 1007
- Rauch T., Reiff E., Werner K., Kruk J.W., 2008, *ASP Conf. Ser.*, 391, 135
- Rauch T., Werner K., Kruk J.W., 2009, *AIP Conf. Ser.*, 1135, 168
- Rauch T., Ziegler M., Werner K., Kruk J.W., Oliveira C.M., Vande Putte D., Mignani R.P., Kerber F., 2007, *A&A*, 470, 317
- Reid W.A., Parker Q.A., 2010, *PASA*, 27, 187
- Reindl N., Ringat E., Rauch T., Werner K., Kruk J.W., 2012, in Manchado A., Stanghellini L., Schönberner D., eds, *Proc. IAU Symp. 283, Planetary Nebulae: An Eye to the Future*. Cambridge Univ. Press, Cambridge, p. 482
- Reindl N., Rauch T., Werner K., Kruk J.W., 2013, *ASP Conf. Ser.*, 469, 143
- Ringat E., Friederich F., Rauch T., Werner K., Kruk J.W., 2011, in *Proc. APN V Conference*, 165
- Roeser S., Demleitner M., Schilbach E., 2010, *AJ*, 139, 2440
- Ruiz N., Chu Y.-H., Gruendl R.A., Guerrero M.A., Jacob R., Schönberner D., Steffen M., 2013, *ApJ*, 767, 35
- Russell S.C., Dopita M.A., 1992, *ApJ*, 384, 508
- Sabbadin F., Minello S., Bianchini A., 1977, *A&A*, 60, 147
- Sabin L. et al., 2013, *MNRAS*, 431, 279
- Saio H., Jeffery C.S., 2002, *MNRAS*, 333, 121
- Schlafly E.F., Finkbeiner D.P., 2011, *ApJ*, 737, 103
- Schlegel D.J., Finkbeiner D.P., Davis M., 1998, *ApJ*, 500, 525
- Schmutz W., Hamann W.-R., Wessolowski U., 1989, *A&A*, 210, 236
- Schönberner D., 1983, *ApJ*, 272, 708
- Schönberner D., Jacob R., Steffen M., Perinotto M., Corradi R.L.M., Acker A., 2005, *A&A*, 431, 963
- Schwarz H.E., Corradi R.L.M., Melnick J., 1992, *A&AS*, 96, 23
- Skrutskie M.F. et al., 2006, *AJ*, 131, 1163
- Smith L.F., Meynet G., Mermilliod J.-C., 1994, *A&A*, 287, 835
- Smith L.F., Shara M.M., Moffat A.F.J. 1996, *MNRAS*, 281, 163
- Smith L.J., Stroud M.P., Esteban C., Vilchez J.M., 1997, *MNRAS*, 290, 265
- Soker N., 1997, *ApJS*, 112, 487
- Soker N., Borkowski K.J., Sarazin C.L., 1991, *AJ*, 102, 1381
- Spitzer L., 1978, *Physical processes in the interstellar medium*. New York, Wiley-Interscience
- Steiner J.E., Diaz M.P., 1998, *PASP*, 110, 276
- Steiner J.E., Oliveira A.S., 2005, *A&A*, 444, 895
- Stock D.J., Barlow M.J., 2010, *MNRAS*, 409, 1429
- Stock D.J., Barlow M.J., Wesson R., 2011, *MNRAS*, 418, 2532
- Stroud M.P., 1997, *ASP Conf. Ser.*, 120, 349
- Thackeray A.D., Webster B.L., 1974, *MNRAS*, 168, 101
- Todt H., Peña M., Hamann W.-R., Gräfener G., 2010a, *A&A*, 515, 83
- Todt H., Peña M., Hamann W.-R., Gräfener G., 2010b, *AIP Conf. Ser.*, 1273, 219
- Todt H., Peña M., Zühlke J., Oskinova L., Hamann W.-R., Gräfener G., 2012, in *Proc. IAU Symp. 283, Planetary Nebulae: An Eye to the Future*. Cambridge Univ. Press, Cambridge, p. 510
- Todt H. et al., 2013, *MNRAS*, 430, 2302 (TK13)
- Torres-Peimbert S., Peimbert M., Ruiz M.T., Peña M., 1993, *Proc. IAU Symp.*, 155, 584
- Tsamis Y.G., Barlow M.J., Liu X.-W., Danziger I.J., Storey P.J., 2003, *MNRAS*, 345, 186
- Tylenda R., Acker A., Stenholm B., 1993, *A&AS*, 102, 595
- Tylenda R., Siódmiak N., Górny S.K., Corradi R.L.M., Schwarz H.E., 2003, *A&A*, 405, 627
- van der Hucht K.A., Jurriens T.A., Wesselius P.R., Olon F.M., The P.S., Williams P.M., 1985, *A&A*, 145, 13
- Vreux J.M., Dennefeld M., Andriat Y., 1983, *A&AS*, 54, 437
- Wachter S., Mauerhan J.C., Van Dyk S.D., Hoard D.W., Kafka S., Morris P.W., 2010, *AJ*, 139, 2330
- Wareing C.J., 2010, *PASA*, 27, 220
- Wareing C.J., O'Brien T.J., Zijlstra A.A., Kwitter K.B., Irwin J., Wright N., Greimel R., Drew, J.E., 2006, *MNRAS*, 366, 387
- Wassermann D., Werner K., Rauch T., Kruk J.W., 2010, *A&A*, 524, A9
- Weidmann W.A., Gamen R., 2011, *A&A*, 531, A172
- Weinberger R., 1989, *A&AS*, 78, 301
- Werner K., 1992, *Lecture Notes in Physics*, 401, 273
- Werner K., 2012, in Manchado A., Stanghellini L., Schönberner D., eds, *Proc. IAU Symp. 283, Planetary Nebulae: An Eye to the Future*. Cambridge Univ. Press, Cambridge, p. 196
- Werner K., Herwig F., 2006, *PASP*, 118, 183
- Werner K., Rauch T., Barstow M.A., Kruk J.W., 2004, *A&A*, 421, 1169
- Werner K., Rauch T., Reiff E., Kruk J.W., 2009, *Ap&SS*, 320, 159
- Wesson R., Stock, D.J., Scicluna P., 2012, *MNRAS*, 422, 3516
- Zacharias N., Monet D.G., Levine S.E., Urban S.E., Gaume R., Wycoff G.L., 2004, *BAAS*, 36, 1418
- Zhang Y., Liu X.-W., Liu Y., Rubin R.H., 2005, *MNRAS*, 358, 457
- Zuckerman B., Aller L.H., 1986, *ApJ*, 301, 772